CHEMICAL MODELING OF ZINC ENZYMES

To Barbara

CHEMICAL MODELING OF ZINC ENZYMES

By

Byron DeLaBarre, B. Sc.

A Thesis

Submitted to the School of Graduate Studies

in Partial Fulfillment of the Requirements

for the Degree

Master of Science

McMaster University

MASTER OF SCIENCE (1995)
(Chemistry)

McMASTER UNIVERSITY
Hamilton, Ontario, Canada

TITLE

CHEMICAL MODELING OF
ZINC ENZYMES

AUTHOR:

Byron DeLaBarre, B.Sc. (University of Waterloo, Waterloo, Canada)

SUPERVISOR:

Dr. C. J. L. Lock

NUMBER OF PAGES:

xiv, 110

ABSTRACT

This work describes efforts towards creating chemical models for a variety of zinc based metalloenzymes. A background on the current progress of modeling zinc enzymes is presented, as is a brief review of zinc biochemistry.

The structure of triaquo(tris-2-pyridylphosphine)nickel(II) dinitrate is presented and compared with its zinc analogue. Both structures have octahedral geometry with no unusual bond lengths.

The synthesis and characterization of bis(2,4,5-tribromoimidazole)(diaquo)zinc(II) (**II**) is also presented in this work. A similar compound, $Zn(Im)_2$ (**III**) was also prepared in this work. Both compounds were characterized by X-ray crystallography, IR spectroscopy, and elemental analysis. Neutron crystallography was used to characterize (**II**) as a peraquo species. Both (**II**) and (**III**) possess tetrahedral geometry about the zinc atom. (**III**) is multiply catenated and cannot be considered as a discrete molecular species.

The pKa_2 of 2,4,5-tribromoimidazole, the organic ligand in (**II**), was measured and found to be 10.7(2).

Bond valence theory was used to analyze (**II**). Extended Huckel molecular orbital calculations were carried out on (**II**). (**II**) was compared with a variety of other zinc-imidazole compounds. It was discovered that (**II**) has unusually small carbon-nitrogen-carbon angles within its tribromoimidazole rings. It is uncertain whether this

feature is because of the coordination of the tribromoimidazole rings to the zinc atom, or whether it is an inherent feature of the tribromoimidazole rings.

A copper analogue of (II) has also been synthesized and has been tentatively assigned the formula $Cu(ImBr_3)_2(OH_2)_2$. X-ray characterization of this compound has not yet been accomplished.

ACKNOWLEDGMENTS

I would like to thank Dr. C. J. L. Lock for his guidance during this work. I would like to thank all of the Lock group members, past and present, for advice and companionship during the course of this work. They are: Dr. Hosein Alarabi, Samantha Bennet, Theresa Fauconnier, Dave Green, Dr. Alan Guest, Daren LeBlanc, Dr. Z. Wang, Dr. Yi Wei, and John Valliant. Thanks also go to Dr. Mike Burnett at Oak Ridge Laboratories for his help with the neutron diffraction studies. I would like to thank Dr. Jim Britten for his help with X-ray diffraction studies. A thank-you to Dr. Pierre Brassard and the members of his group for their help with the pKa studies. Finally, the financial support from the Department of Chemistry at McMaster University has been appreciated.

Table of Contents

LIST OF FIGURES

LIST OF TABLES

1. INTRODUCTION AND BACKGROUND

1.1 Introduction

This work was designed to examine first row transition metal complexes of tripod-style ligands (see section 1.2.4 below). This built upon previous work in our laboratory[1], designed to model the structure and function of metalloenzymes.

The first complex examined was a nickel compound, tris(1-methyl-2-ethyl-imidazole)phosphine nickel(II), which we were unable to characterize properly. Further studies on the structure of a different, but related compound [triaquo(tris-2-pyridylphosphine)nickel(II) dinitrate] yielded better results, but in the course of our research, we discovered a simple ligand (2,4,5-tribromoimidazole) (**I**) (see section 1.2.5 below). (**I**) forms a complex with aqueous zinc(II) in basic solution to produce bis(2,4,5-tribromoimidazole)(diaquo)zinc(II), (**II**), which we soon realized to be a unique and potentially useful model for a variety of zinc enzymes. If zinc(II) is mixed with imidazole under the same conditions, a multiply catenated structure with the formula $Zn(Im)_2$ (**III**), is formed. (**I**) also forms a complex with aqueous copper (II) (**IV**) in basic solution, but characterization of the compound is incomplete.

The synthesis of (**II**), several of its analogues, and the characterization of these compounds by a variety of methods is the main focus of this thesis. Some theories regarding the stability of (**II**) are presented. A comparison between the structural features of (**II**) and relevant compounds is made. The implications of the structure of (**II**) towards understanding zinc enzyme mechanisms are discussed. This thesis also presents the X-ray structures of the nickel compounds mentioned previously. The solved structure of [triaquo(tris-2-pyridylphosphine)nickel(II) dinitrate] is presented and compared with a zinc analogue previously characterized by Mary Turner (see Reference 1).

The following sections outline our philosophy towards enzyme modeling with particular regard to modeling zinc enzymes. Also, a brief review of zinc physiology and biochemistry is included to make the reader more aware of the importance of this metal in biological processes.

1.2 Building Chemical Models of Enzymes

1.2.1 Advantages of Chemical Models

When exploring the mechanism of enzymes, it is often useful to synthesize chemical models of the active sites. This approach has several advantages.

(a) The characterization of small molecules by X-ray diffraction is much simpler than the characterization of macromolecules, allowing a higher resolution picture of the atomic structure.

(b) It is easier to make derivatives in order to probe the mechanism.

(c) The solubility of the model compound will likely be different from the solubility of the enzyme, allowing a wider range of experiments to be performed.

(d) The spectroscopic characterization of the model compound is likely to be less vague than spectroscopic observations of the macromolecule.

(e) In developing the chemistry and techniques necessary to model enzyme active sites, new compounds and areas of research may be discovered, and our understanding of the chemistry of the metal atoms will be enhanced.

1.2.2 Disadvantages of Chemical Models

There are, however, some drawbacks to the use of model compounds. Two potential and related difficulties are outlined below. Both problems are an elaboration of the obvious fact that the model compounds are not, by definition, the actual enzyme.

(a) The model compound may oversimplify the chemistry that occurs at the active site. For instance, the interaction of residues not directly bound to the metal atom may not be taken into account. The unique environment created in the active site of the protein will not be reproduced precisely; important differences may arise between the chemistry of the model compound and the chemistry of the enzyme. If these differences are not taken into account, erroneous conclusions about the enzyme mechanism may be the result. The defense against this problem is to take as many approaches as is possible by creating a large variety of compounds which mimic the structure and chemistry of the enzyme.

(b) Active site models may have solubility or stability problems. These difficulties will limit the experiments which may be performed and thus the utility of the compound as a model for the enzyme. The solution to this problem is to effect slight variations in the structure of the models; however, this solution creates another problem: a widening of the difference between the model and the active enzyme. It has often been noted by scientists who choose to take the approach of model building that the most appropriate models are often the most difficult to synthesize!

1.2.3 Zinc Enzyme Model Categories

Models for zinc enzymes can be divided into three main categories: tripod ligands, simple ligands, and polyamine macrocycles. An excellent review of zinc coordination chemistry relevant to active site model building has been written by R. H. Prince[2].

1.2.4 Tripod Ligands

The tripod ligands can be described as having three ligating groups joined by a central atom. The central atom can be nitrogen, boron, carbon, or phosphorus. The ligating group is typically a nitrogen heterocycle. Some examples are shown below in Figure 1.2.4.

Figure 1.2.4 - Examples of Tripod Ligands

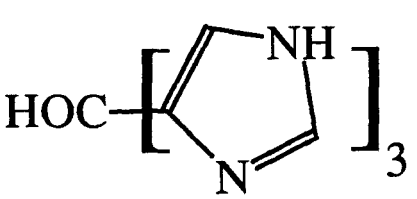

A

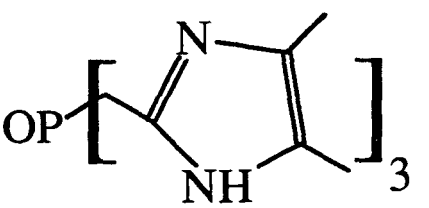

B

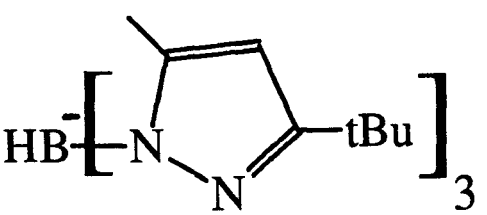

C

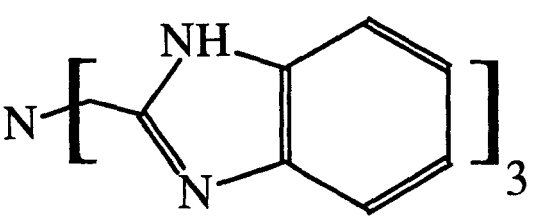

D

Compound A in Figure 1.2.4 was synthesized by Breslow *et al.*[3] and formed a 1:1 complex with zinc with a binding $pK_{Zn(II)}$ of 8.47. A 1:1 zinc complex with compound B in

Figure 1.2.4 was prepared by Brown *et al.*[4] and showed a $pK_{Zn(II)}$ value of 6.00. The $pK_{Zn(II)}$ for both carbonic anhydrase and carboxypeptidase is 10.5. A zinc hydroxy complex of compound C in Figure 1.2.4 was synthesized and characterized by single crystal X-ray diffraction by Looney *et al.*[5]. Looney's complex reacted instantly with CO_2 in benzene to produce a carbonato complex as characterized by IR spectroscopy. The zinc complex of compound D in Figure 1.2.4 was synthesized and characterized by Thompson *et al.*[6].

Tripod ligands take advantage of the chelate effect to form stable tetrahedral zinc species. Unfortunately, the cost of employing the chelate effect is stereochemical rigidity; this is a high price to pay if consideration is to be given to the putative tetra to penta coordination change which has been invoked to explain the ubiquity of zinc in enzymes. Also, the solubility and/or stability of the metal complexes with the tripod ligands in water is often poor.

1.2.5 Simple Ligands

The initial efforts in trying to understand the chemistry of biological zinc consisted of studies of zinc complexes of imidazole, substituted imidazoles, histidine, and related ligands. The ligating groups of simple ligands are not joined by a central atom nor are they linked as a macrocycle. These systems are chemically simple in comparison with the

other two approaches towards modeling zinc enzymes, yet a great deal of effort has been applied towards trying to understand them. That is because they represent, at least structurally, the most accurate models of the metalloenzyme active site.

These compounds do not have the advantage of the chelate effect for the formation of stable complexes; it is difficult to obtain well defined coordination numbers, especially lower ones (two, three, or four), with zinc complexes in solution. An excellent study of aqueous zinc imidazole chemistry has been carried out by Sigel and Martin[7].

Sigel and Martin also showed that the characterization of zinc (II) complexes in the solid state contrasts with the characterization of zinc (II) complexes in aqueous solution. A recent evaluation of 490 crystal structures showed that divalent zinc has coordination of four in 58% of the complexes. Coordination numbers five and six were found for 13% and 27% of the complexes, respectively.

In terms of zinc-imidazole compounds, the imidazole molecule (or imidazole derivative) can bind as neutral imidazole, in which case the doubly positive charge on zinc must be balanced by two anions, as in (dichloro)(diimidazole)zinc(II)[8]. Imidazole can also occur as a mixture of neutral and anionic ligands, as in the $\{Zn(imidazole)_2(imidazolate)_1\}(NO_3)$ compound[9]. $\{Zn(imidazole)_2(imidazolate)_1\}(NO_3)$ comprises both terminal and bridging imidazole ligands (the neutral imidazole ligands are

terminal whereas the imidazolate ligands are bridging). The bridging imidazolate motif is also displayed in $Zn(Im)_2$, first characterized by Lehnert and Seel[10] and accidentally reproduced in this thesis work. The zinc imidazole chains form a multiply catenated species, in which the zinc atoms are all tetrahedrally coordinated by the nitrogen atoms of the imidazolate ligands.

Despite the extensive characterization of zinc compounds with simple ligands, no aquo species of imidazole coordinated zinc atoms have been characterized until now. Such a species would be helpful towards understanding the enzyme mechanism, as the imidazole groups would not be held in place with artificial links. It is assumed that the histidine residues have a fair degree of flexibility within the active site of the zinc enzymes, and thus it is likely that the complete zinc(II) site environment dictates the coordination geometry.

1.2.6 Nitrogen Macrocycles

Zinc (II) complexes with nitrogen macrocycles do not suffer from the solubility and stability problems of the tripod ligands. Two examples of nitrogen macrocycles are shown in Figure 1.2.6 below.

difficulty of accurately locating hydrogen atoms by X-ray analysis, the hydrogen atom positions could not be determined directly from the crystallographic data. The assignment of the hydrogen atoms and thus the formulation of the compound as a hydroxide species rather than an aquo species is suspect.

Like the tripod ligands, the macrocycles take advantage of the chelate effect to form strong complexes with zinc. They are fairly simple to synthesize and thus it is easy to make systematic variations of the ligand structure in order to probe the coordination geometry of the zinc atom and its effect on catalysis. The complexes are stable and soluble in aqueous solution. Unfortunately, the environment around the zinc atom is only nominally similar to the distorted tetrahedral coordination found around the zinc atoms in enzymes (see Sections 1.7 and 1.9 for a description of zinc coordination geometry in enzymes).

Despite the only slight similarity between the model and an enzyme such as carbonic anhydrase (see Section 1.10 for a description of this enzyme), the pKa value of the bound water atom in $Zn(II)(OH_2)12[ane]N_3$ is very close to that of carbonic anhydrase. The bound water molecule has a pKa of 8.7 compared to a pKa of 7.3 for CA. Also, the affinity constants for a series of ions ($OH^- > CH_3CO_2^- > SCN^- > I^- > Br^- > Cl^- > F^-$) show trends similar to those for carbonic anhydrase (the thiocyanate and acetate ions switch places in the order for carbonic anhydrase). With regards to catalysis, the second

order rate constant value for the hydration of acetaldehyde (this value is technically easier to obtain then the value for the hydration of carbon dioxide) by $Zn(II)(OH_2)12[ane]N_3$ is approximately 200 $M^{-1}s^{-1}$, which is one seventh the value determined for carbonic anhydrase. The large discrepancy has been attributed to the overall difference in the zinc environment in the model compound and the actual enzyme; the enzyme will have hydrophobic pockets which may very well help to bind the substrate initially and then eject it after catalysis. As previously discussed in Section 1.2.2, this difference is an inherent problem with any chemical model of an enzyme active site.

The $Zn(II)(OH_2)12[ane]N_3$ complex also shows activity towards carboxylate and phosphate substrates, making it a viable model for enzymes like carboxypeptidase and alkaline phosphatase. Despite their minimal structural resemblance to the biological archetypes, the nitrogen macrocycles have been the most successful ligands for modeling the zinc enzyme active sites. Their success is likely caused by a combination of the stability given by the chelate effect with the flexibility afforded by the macrocyclic structure. The stability, solubility, and relatively easy synthesis of these ligands have made them a vast improvement over the tripod ligands.

1.3 Natural Abundance of Zinc

The body uses several first row transition and group IIB elements such as iron, manganese, copper, and zinc. Of these four metals, zinc is the most widely used in

biological systems. The special role of zinc in living organisms is highlighted by its moderate abundance in nature: at 0.02 weight percent, it is the 27th most abundant element in the earth's crust. This can be compared to iron (4.2 weight per cent), manganese (0.1 weight per cent), and copper (0.01 weight per cent)[13].

1.4 Zinc in the Body

A healthy adult human body weighing 70 kg contains 2 to 3 grams of zinc[14]. The daily requirement of zinc for that same human is in the range of 10-15 mg/day and is increased up to 25 mg/day for pregnant women[15]. The body loses approximately 5 mg/day of zinc through excretion, urination, sweat, and the sloughing of dead skin cells[16].

More than 99% of bodily zinc is intracellular[17] and tightly bound into proteins. The remaining zinc can be found in the blood serum, bound mainly to what is thought to be albumin, a transport protein.[18] Particularly high concentrations of zinc are found in the eye, the hippocampus, the prostate, prostatic secretions, and sperm[19].

1.5 Zinc Pathology

Subjects deficient in zinc show a wide range of symptoms including lethargy, rough skin, absent pubic and auxiliary hair, hypogonadism, undescended testes, dwarfism, and hepatosphlenomegaly[20]. Pathogenesis from zinc excess is virtually nonexistent: brass chills (resulting from the inhalation of zinc during the smelting process) is the only well established toxic manifestation of zinc. The disease is never fatal and is completely

reversible upon removal of the zinc fumes[21]. Zinc is the only pre-, post-, or transitional metal that is essentially nontoxic[22].

A recent exception to the lack of zinc toxicity was revealed by the clinical findings of Masters *et al.*[23] who showed that zinc supplements exacerbated the symptoms of Alzheimer's disease in a handful of patients. These findings were substantiated by the work of Tanzi[24] *et al.* who reported that physiological levels of zinc could induce tinctorial amyloid formation in solutions of human $A\beta_{1\text{-}40}$ protein. The formation of Aβ amyloids in the neural tissue of subjects suffering from Alzheimer's disease has been well established; however, it is still not certain whether the amyloids are a symptom or a cause of the disease. Tanzi's result was underscored by his discovery that the same conditions will not induce amyloid formations in rat $A\beta_{1\text{-}40}$ solutions. Rats are immune to the formation of the brain amyloids characteristic of Alzheimer's disease.

1.6 Zinc Proteins

Obviously, zinc is an important biological metal. Biological zinc is found exclusively as the divalent cation and, as mentioned above, nearly all (99%) of zinc is bound into proteins. Examples of zinc enzymes can be found in all six enzyme classes (oxidoreductases, transferases, hydrolases, lyases, isomerases, and ligases). A survey of these enzymes from Vallee and Falchuk's excellent review[25] on zinc physiology is

reproduced in Table 1.6 below. Note that in approximately one third of the known zinc containing enzymes, the role of the zinc atom has not yet been determined.

Table **1.6** - Zinc Enzymes

Name	Source	Role*	Name	Source	Role
Class I (Oxidoreductases)			***Class III (Hydrolases)***		
Alcohol Dehydrogenase	yeast, vertebrates, plants	c, s	Leukotriene A_4 hydrolase	human	c
Sorbitol dehydrogenase	vertebrates	c	Alkaline phosphatase	mammals, bacteria	c, ca
D-Lactate dehydrogenase	barnacles, bacteria	?	5'-Nucleotidase	bacteria, lymphoblast, plasma	?
D-Lactate cytochrome reductase	vertebrates, plants	ca	Phosphodiesterase	snake venom	c
Superoxide Dismutase	fungi, bacteria	?	Nuclease	microbes	?
Class II (Transferases)			Aminopeptidase	mammals, fungi, bacteria	c, ca
Transcarboxylase	*P. shernamii*	?	Astacin	crustacea	c
Aspartate transcarbamylase	*E. coli*	s	Thermolysin	bacteria	c
Phosphoglucomutase	yeast	?	Carboxypeptidase	vertebrates, crustacea, plants, bacteria	c
RNA polymerase	wheat germ, bacteria, viruses	c	Elastase	*P. aeruginosa*	c
Reverse transcriptase	oncogenic viruses	c	Collagenase	mammals, bacteria	c
Nuclear poly (A) polymerase	rat liver, virus	c	β-Lactamase II	*B. cerus, P. maltophila*	c

*c= catalytic, ca=cocatalytic, s=structural, ?=unknown (see Section 1.9)

Continuation of Table 1.6 - Zinc Enzymes

Name	Source	Role[†]	Name	Source	Role
Class IV (Lyases)			***Class V (Isomerases)***		
Fructose-bisphosphate aldolase	yeast, bacteria	c	Phosphomannose isomerase	yeast	?
1-Rhamnulose-1-phosphate aldolase	*E. coli*	c	DNA topoisomerase I	*E. coli*	?
Carbonic Anhydrase	animals, plants	c	***Class VI (Ligases)***		
Glyoxalase I	mammals, yeast	c	tRNA synthetase	*E. coli, B. stearothermophilus*	c
			Pyruvate carboxylase	yeast, bacteria	?

1.7 Zinc Ligation

Biological zinc is typically bound to sulfur atoms (cysteine residues), oxygen atoms (water, aspartic acid, glutamic acid), but is most often bound to the nitrogen atoms of the histidine residue (see Figure 1.7 for the structures of the amino acids mentioned). A survey of the ligation to biological zinc atoms can be found in Vallee and Falchuk's review on zinc physiology and is reproduced in Table 1.7 below.

[†] c= catalytic, ca=cocatalytic, s=structural, ?=unknown (see Section 1.9)

Figure 1.7 Amino Acids which Bind to Zinc

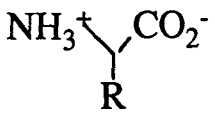

General Amino Acid

R=

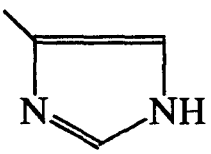

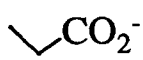

Histidine (His) **Aspartate (Asp)** **Glutamate (Glu)** **Cysteine (Cys)**

Table 1.7 Ligation of Zinc in Selected Enzymes

Enzyme	Ligand 1	Ligand 2	Ligand 3	Ligand 4
Alcohol Dehydrogenase	Cys	His	Cys	H_2O
Alcohol Dehydrogenase[‡]	Cys	Cys	Cys	Cys
Carboxypeptidase A/B	His	Glu	His	H_2O
Thermolysin	His	His	Glu	H_2O
B. Cereus Neutral Protease	His	His	Glu	H_2O
Carboxypeptidase D	His	His	His	H_2O
β-Lactamase	His	His	His	H_2O
Phospholipase C	His	Glu	His	H_2O
Alkaline Phosphatase	Asp	His	His	H_2O
Carbonic Anhydrase I and II	His	His	His	H_2O

[‡] The first entry is for the catalytic zinc site while the second listing is for the structural zinc site

1.8 Chemical Properties of Zinc

There are several properties of zinc which make it an important metal in biological systems.

(a) Under physiological conditions, it will not undergo redox reactions (divalent zinc is a d^{10} ion).

(b) It is an amphoteric ion and can exist as either an aquo or a hydroxo ion at physiological pH (approximately 7).

(c) Because the d-orbitals of zinc are full, it has a variable coordination sphere and is able to adopt a large variety of coordination geometries. The typical coordination number of biological zinc ranges from four to six and it displays all of the coordination geometries available within this range (tetrahedron, trigonal bypyramid, square pyramid, and octahedron).

(d) The flexibility of the zinc coordination sphere allows it to submit to the stereochemical demands of its environment, giving it a wide variety of chemical activities. Protein structures affect the chemistry of bound zinc as much as zinc, in turn, affects the conformation and adaptability of these large macromolecules.

1.9 Zinc Motifs in Proteins

Zinc atoms in proteins can be divided into four categories: catalytic, cocatalytic, structural, and zinc in metallothioneins.

1.9.1 Catalytic Zinc Sites

Catalytic zinc atoms are necessary for the enzyme to function - they are directly involved in the catalytic process. Two examples of enzymes with catalytic zinc atoms are carboxypeptidase and carbonic anhydrase. The former has catalytic properties towards macromolecules (it cleaves C-terminus residues) whereas the latter has catalytic properties towards small molecules (it catalyzes the interconversion between carbon dioxide and the bicarbonate anion). In both cases, the bound zinc atom is in the active site of the enzyme. Catalytic zinc is generally ligated by two or three histidine residues in a tetrahedral geometry with water always occupying one of the vertices of the tetrahedron.

1.9.2 Cocatalytic Zinc Sites

Cocatalytic zinc atoms exist in close proximity to other zinc or magnesium atoms. The metal atoms are usually ligated by histidine residues and are bridged by aspartic or glutamic acid residues. These metal clusters then act as a catalytic unit. Examples of enzymes with cocatalytic zinc sites include alkaline phosphatase, which contains two zinc atoms and one magnesium atom at its active site; and leucine aminopeptidase, which has

two zinc atoms at its active site. The former catalyzes the hydrolysis of phosphate esters, whereas the latter is responsible for the cleavage of N-terminus peptide bonds. Cocatalytic zinc atoms are not indispensable for enzyme activity or stability[26].

1.9.3 Structural Zinc Sites

Structural zinc atoms are, as the name implies, responsible for enzyme structure. They do not play an active catalytic role, but rather stabilize the tertiary and quaternary structure of the protein in which they are found. An important example of a structural zinc site is alcohol dehydrogenase. Alcohol dehydrogenase is the enzyme which allows the body to process ethanol by converting it into acetaldehyde. The enzyme contains both a catalytic and a structural zinc site with the structural zinc atom bound tetrahedrally by four cysteine residues.

Another interesting example of a structural zinc site is revealed upon examining zinc's role in genetic processes. Several nucleoproteins directly involved with the replication and transcription of DNA have been shown to contain structurally important zinc atoms. A common motif in these proteins (as exemplified by Transcription Factor IIIA[27]) is the tetrahedral ligation of zinc by conserved cysteine and histidine ligands. This results in a loop containing the DNA binding domain of the protein in the sequence between the ligating cysteine and histidine residues. This is commonly referred to as a zinc finger[28]. Up to 500 nucleoproteins are thought to contain zinc as an integral part of their structure.

1.9.4 The Metallothioneins

Metallothionein was first isolated as a cadmium and zinc-containing species[29]. It contains 7 gram atoms of zinc or cadmium per mole of protein and has a primary structure which is thirty per cent cysteine residues. Metallothioneins containing copper, iron, and mercury have also been isolated. The function of metallothionein is not yet completely known, but it is thought to play a role in removing heavy metals from the body, stabilizing membranes, scavenging for radical ions[30] and regulating zinc and copper metabolism.

1.10 Carbonic Anhydrase

To illustrate how zinc can assist a biological process, we will now take a detailed look at the enzyme carbonic anhydrase. Carbonic anhydrase is found in both plants and animals, and its only known biological function is to catalyze the interconversion of CO_2 and HCO_3^-, as shown below in Equation (1.10).

$$CO_2 + H_2O \rightleftharpoons H^+ + HCO_3^- \qquad \text{Equation 1.10}$$

As shown in Table 1.7, the active site of carbonic anhydrase consists of a divalent zinc atom bound tetrahedrally to three histidine residues and one water molecule. This information was obtained from X-ray diffraction. Two other residues in the active site,

neither of which are bound directly to the zinc atom are threonine (Thr-199) and glutamine (Glu-106). Thr-199 and Glu-106 play an important role in the hydrogen bonding network of the active site by acting as a proton shuttle[31]. There are also several water molecules in the active site which are considered to be of functional importance[32].

The pKa value of about 7 for carbonic anhydrase results from the deprotonation of a species in the active site of the enzyme. Many candidates for the acidic species have been suggested, including a zinc bound imidazole group, but the consensus is that it is a water molecule bound to the zinc atom[33].

The role of the zinc bound molecule has been supported by *ab initio* calculations which show that the deprotonation of zinc bound water is more favorable than either the deprotonation of zinc bound imidazolium or that of imidazole itself[34]. The use of *ab initio* and semi-empirical approaches to modeling the enzyme mechanism has been justified on the basis that there are very few solvent molecules in the active site, making the process similar to a gas phase reaction.

The above results have been used to reject any mechanisms which involve the deprotonation of an imidazolium ion rather than a zinc bound water atom. By rejecting such mechanisms, workers have come to the conclusion that the role of zinc is to reduce the pKa of bound water by electrostatic interaction, while at the same time allowing the

hydroxyl group to retain sufficient nucleophilic character to attack CO_2. This mechanism is depicted in Figure 1.10.

Figure 1.10 - Carbonic Anhydrase Mechanism[35]

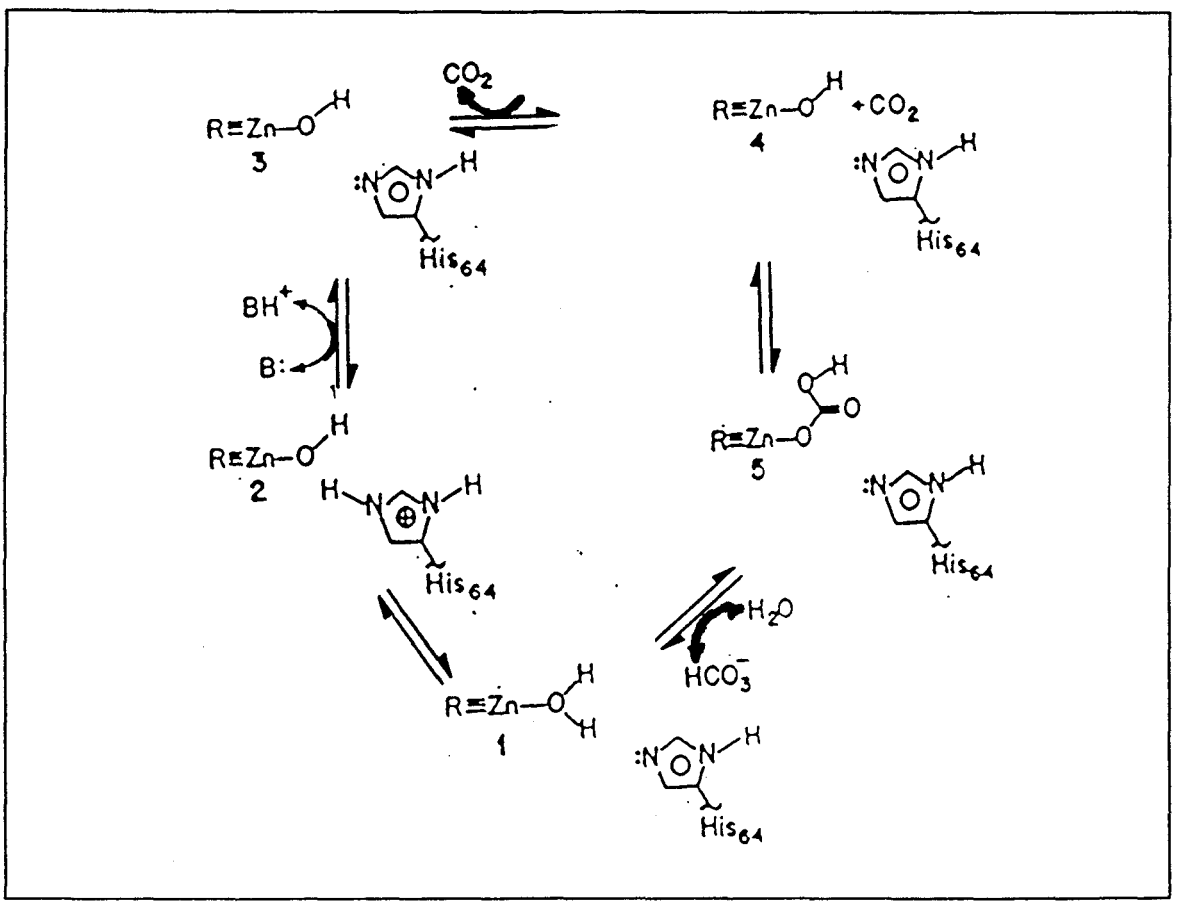

As shown in Figure 1.10, the zinc-water (**1**) species is first deprotonated, followed by a nucleophilic attack upon CO_2 by the resulting zinc-hydroxide species (**3**), forming the zinc-bicarbonate complex (**5**). The bicarbonate anion is then displaced by the water molecule(s) contained in the carbonic anhydrase active site, reforming **1**, from which the catalytic cycle continues. Solvent isotope studies of carbonic anhydrase have shown that

at high buffer concentrations (which mimic physiological pH) the likely rate determining step in this catalytic cycle is the intramolecular proton transfer from **1** to a proton acceptor (possibly a water molecule or a non-zinc bound imidazole molecule such as His-64) in the active site (**1→2**). At lower buffer concentrations the intermolecular proton transfer is rate determining (**2→3**). The effect of buffer upon the enzyme mechanism has been discussed by Silverman and Lindskog[36]. Once the intramolecular proton transfer is complete, the proton is then transferred from the proton acceptor to a buffer in the surrounding medium (**2→3**).

For the formation of the zinc-bicarbonate species, two basic mechanisms have been proposed: in the first the oxygen atom attacks the carbon atom of CO_2 directly (an outer sphere mechanism) while the second has the CO_2 oxygen atom coordinating to the zinc atom followed by an attack of the oxygen atom of **2** (an inner sphere mechanism).

Finally, the loss of the bicarbonate anion is thought to be facilitated by a water molecule in the carbonic anhydrase active site and by a simultaneous loss, from the water molecule, of a proton to a residue in the enzyme, which then completes the catalytic cycle by regenerating **1**.

2. EXPERIMENTS

2.1 Crystallography

Single crystal X-ray and neutron crystallography were the major analytical tools used in this work to characterize the compounds being studied. The experimental details regarding neutron crystallography are presented in Section 2.3. This section gives the experimental details regarding X-ray crystallography. The theoretical basis of single crystal X-ray crystallography is discussed briefly and has been treated in detail by Buerger[37], Luger[38], and Stout and Jensen[39].

2.1.1 Crystal Preparation

The crystals for the diffraction experiments were obtained by a slow evaporation of the reaction medium (up to two weeks). Because of the insoluble nature of the compounds studied in the course of this work, recrystallizations were not attempted.

The dimensions of the crystals chosen for the diffraction experiments ranged from 0.02 mm to 0.5 mm. Crystals of this size will provide adequate diffraction intensity and are uniformly bathed by the incident X-ray beam. The quality of the crystals chosen for a diffraction experiment were judged according to cleanness, uniformity, and extinction

property. Sharp, complete extinction upon each 90° rotation of the crystal under crossed polarizers should be observed for single crystals which do not have a three fold axis as a symmetry element. The crystals chosen were mounted on a 0.05mm to 0.2mm diameter glass pins with epoxy cement.

Crystal densities were measured by suspending the crystals in a mixture of two miscible liquids, one less and one more dense than the crystal. The measurements were performed in triplicate and typically had errors less than ± 0.005 g·ml^{-1}. Literature values are typically quoted with an error range of ± 0.02 g·ml^{-1}.

The observed density of the crystal (ρ_{obs}) was compared to the calculated density of the crystal (ρ_{calc}). Equation 2.1.1 shows how ρ_{calc} was calculated

$$\rho_{calc} = (M)(Z)/(0.6022)(V) \quad (g)(cm^{-3}) \qquad \text{Equation 2.1.1}$$

where M is the gram molecular weight, Z is the number of molecules in a unit cell, and V is the volume of the unit cell in cubic angstroms. Good agreements between ρ_{obs} and ρ_{calc} were observed for the compounds studied in this work.

2.1.2 Data Collection

Unit cell determination and intensity data collection were performed on a Nicolet P3 diffractometer. The diffractometer was controlled through software run on a Vax workstation running P3 softwear. Crystals were centred optically and, if possible, with the longest axis aligned close to the ω-2θ axis on the diffractometer, in order to minimize errors in absorption correction.

The incident beam was generated by a Ag X-ray tube with power settings at 25 kV and 15 mA. The beam was passed through a graphite monochromator (to isolate the K_α peak (λ=0.56086 Å) and then through a collimator in order to get a beam of uniform dimensions.

A random search of reciprocal space was performed to find 25-30 reflections. A search for possible supercells was done automatically. The determination of accurate cell parameters, the orientation matrix, and the Laue group were also done automatically. The resulting information was used to drive the diffractometer to appropriate angles for hkl data collection.

Intensities were measured with a scintillation counter and then passed onto a Sun computer for processing. Individual reflections were measured with either an ω scan or a

θ,2θ scan (only one type of scan was used for any one specimen) to avoid intensity overlap between neighbouring reflections.

An upper value of 2θ was selected based on the diffracting power of the crystal. Scans were made from 1.0° below the $K_{\alpha 1}$ position to 1.0° above the $K_{\alpha 2}$ position. The scan rate for each reflection was determined by the diffractometer software.

Two or three check reflections were chosen to be measured every 97 reflections. The check reflections were used to monitor both the instrument and crystal stability.

Absorption corrections were accomplished by either the ψ-scan[40] or the Gaussian technique[41]. The indexing of individual crystal faces for the Gaussian technique was accomplished by optically aligning the crystal face perpindicular to the incident beam and then cross-referencing the diffractometer settings to previously indexed values. The crystal dimensions (for the ψ-scan) and the dimensions of individual crystal faces (for the face-indexing) were measured with the use of a microscope connected to a television monitor which was calibrated with a standard ruler.

More details about data collection can be found in the Nicolet P3 diffractometer manual[42].

2.1.3 Structure Solution and Refinement

The scattering factor of an atom (f) is shown in Equation 2.1.3(a).

$$f=f_o\exp[-B(\sin^2\theta)/\lambda^2] \qquad \text{Equation 2.1.3(a)}$$

where f_o is the scattering factor of a spherical atom and is a function of atom type and $[\sin\theta/\lambda]$. Values of f_o against $[\sin\theta/\lambda]$ for all stable elements have been tabulated with anomalous dispersion corrections[43]. B is the temperature factor, which is related to the mean-square amplitude of atomic vibration.

For a crystal with a known structure, the structure factors can be calculated (F_c) for each reflection at hkl, according to Equation 2.1.3(b).

$$F_c(hkl)=\Sigma f_j\exp[2\pi i(hx_j+ky_j+lz_j)] \qquad \text{Equation 2.1.3(b)}$$

where f_j is the scattering factor of the jth atom, and x_j, y_j, z_j are the positional parameters of that atom. The sum is done over all atoms in the unit cell.

If all of the structure factors of the hkl reflections are known, the electron density (ρ) at any point (x,y,z) inside the unit cell can be calculated by a Fourier synthesis, as shown in the two equivalent expressions Equation 2.1.3(c) and Equation 2.1.3(d).

$$\rho(x,y,z)=(1/V)\ \Sigma\Sigma\Sigma F_{hkl} \exp[-2\pi i(hx+ky+lz)] \qquad \text{Equation 2.1.3(c)}$$

$$\rho(x,y,z)=(1/V)\ \Sigma\Sigma\Sigma \left| F_{hkl} \right| \exp[-2\pi i(hx+ky+lz-\alpha_{hkl})] \qquad \text{Equation 2.1.3(d)}$$

where V is the volume of the unit cell, and α_{hkl} is the phase angle. The summations are done over all h,k, and l.

In practice, it is the moduli of the structure factors, $\left| F_{hkl} \right|$, that are observed. Phases for each reflection have to be determined. The direct method was used in this work to determine the phases associated with the individual structure factors.

The direct method uses probability to assign phases directly to a series of related reflections. The relation among the reflections is that the indices of one of them must be expressible as the sum of the indices of the other two. In practice, it is only necessary to phase about 10% of the reflections (the strongest reflections are used) to obtain a

recognizable picture of the molecular structure. The phases of the F_c values are assigned to the corresponding F_o values. An improved solution is obtained after another Fourier synthesis which uses all of the assigned F_o values. A complete structure solution is obtained from difference Fourier syntheses. The difference Fourier syntheses were carried out after least squares refinement of positional, occupational, and thermal parameters. The difference Fourier synthesis results in unassigned peaks of electron density ($\Delta\rho$), as shown in Equation 2.1.3(e)

$$\Delta\rho=(1/V)\,\Sigma\Sigma\Sigma\,(\,|F_o|\,-\,|F_c|\,)\exp[-2\pi i(hx+ky+lz-\alpha_c)] \quad \text{Equation 2.1.3(e)}$$

where α_c is the phase determined for F_c. Missing atoms appear as postive peaks in the difference map; improperly assigned atoms appear as negative peaks.

Raw structures were refined by the method of least-squares. Refinements were done against F^2 values. Refining against F^2 values allows all reflections with $I > -3\sigma_I$ to be used during the refinement stages. Full-matrix least-squares minimized the function shown in Equation 2.1.3(f).

$$\Sigma\omega(\,|F_o|^2\,-\,|kF_c|^2)^2 \quad \text{Equation 2.1.3(f)}$$

where ω is an overall scaling factor and k is a scaling factor necessary to avoid false minima. The summation is over all hkl. Atomic positional parameters, site occupancy factors, temperature factors, and the overall scaling factor were varied. A difference Fourier synthesis was performed after each refinement. Peaks from the difference map can guide the refinement towards the most accurate solution. This process is repeated until all of the parameters effectively cease to vary, and the difference map is essentially flat. The quality of the final solution can be judged according to the R, R_w, and S values shown in Equations 2.1.3(g-i). The R value is calculated for F, usually with a cutoff of between two and four sigma. The R_w value is calculated for F^2 and is generally twice the value of R.

$$R = \Sigma (|F_o| - |F_c|) / \Sigma |F_o| \qquad \text{Equation 2.1.3(g)}$$

$$R_w = [\Sigma w (|F_o|^2 - |F_c|^2)^2 / \Sigma |F_o|^2]^{1/2} \qquad \text{Equation 2.13(h)}$$

$$S = [\Sigma w (|F_o|^2 - |F_c|^2)^2 /(M-N)]^{1/2} \qquad \text{Equation 2.1.3(i)}$$

where w is the weight, M is the number of observed reflections and N is the number of parameters refined. The sums are over all reflections.

Further details about structure solution and refinement can be found in the references mentioned above.

2.2 Experimental Details Regarding Individual Samples

2.2.1 Triaquo(tris-2-pyridylphosphine)nickel(II) dinitrate

X-ray quality crystals for triaquo(tris-2-pyridylphosphine)nickel(II) dinitrate were grown by recrystallization from a water/methanol mixture. Triaquo(tris-2-pyridylphosphine)nickel(II) dinitrate crystallizes with one molecule of water. The crystal was mounted on a glass pin for data collection. Unit cell parameters were refined by a least-squares fit of 40 reflections at 2θ angles between 14.47° and 32.97°. A psi-scan was made to correct for absorption problems, with the approximation that the crystal was an ellipsoid. An ω scan was used to obtain intensity data. The structure was solved by direct methods. The space group was initially chosen to be $P2_1/n$ based on systematic absences and a Wilson test which indicated that the space group was likely centrosymmetric. A second solution was done in $P2_1$ (a non-centrosymmetric space group) to help model disorder problems in the nitrate molecules, the ring carbon atoms, and the coordinated water molecules. This resulted in two identical molecules of triaquo(tris-2-pyridylphosphine)nickel(II) dinitrate in the asymmetric unit. There was a high correlation (approximately 0.9) between the positional and thermal parameters of the two molecules during the refinement. Hydrogen atoms were placed in calculated positions with fixed temperature factors. Scale, positional parameters, and the anisotropic temperature factors for the remaining atoms were varied to minimize the least squares function (Equation

2.1.3(e)). Because of a slight disorder problem with the coordinated oxygen atoms, the anisotropic temperature factors of two of the coordinated oxygen atoms were restrained to make the U_{ij} factors approximate isotropic behaviour (O2 and O3). Further details regarding the specimen, the data collection and refinement are given in Table 2.2.1.

Table 2.2.1

Crystallographic Parameters forTriaquo(tris-2-pyridylphosphine)nickel(II) dinitrate

Formula / Formula weight	$C_{15}\ H_{20}\ N_5\ Ni\ O_{10}\ P$ / 520.04
Crystal colour / shape / size (mm)	purple / needle / 0.22 X 0.22 X 0.84
Space Group	$P2_1$
Incident Radiation (Å)	Ag K_α (0.56086)
Unit cell parameters (Å and degrees)	a = 8.978(2) b = 16.748(3) c = 13.919(3)
	$\alpha = 90.00\ \beta = 91.90(3)\ \gamma = 90.00$
Volume ($Å^3$) / Z	2091.8(7) / 4
ρ_{calc}	1.651
2θ Range (degrees)	$3.6 \leq 2\theta \leq 50.28$
Indices Range	$-1 \leq h \leq 13, -1 \leq k\ 25, -21 \leq l \leq 21$
Temperature (°C)	22(1)
Absorption coefficient (mm^{-1})	0.564
Transmission factor range	0.683-0.718
Standards / Decay	3 standards checked every 97 measurements
	varied from 0.9817 to 1.0012
# of Reflns Measured / # of Unique Reflns	9595 / 8265
R_{int}	0.041
F(000)	1072
# of Parms for Refinement / # Restraints	577 / 13
R / R_w	0.045 / 0.097
Final $\Delta\ \sigma^{-1}$ -- Maximum / Average	1.050 / 0.141
Final Difference map -- Max / Min (e $Å^{-3}$)	0.31 / -0.30
Weighting	$w= [\sigma^2(F_o^2)+(0.0300P)^2P]^{-1}\ \ P=(F_o^2+2F_c^2)^3$
S	0.78

2.2.2 Bis(2,4,5-tribromoimidazole)diaquozinc(II)

Crystals were grown over a two week period by allowing the reaction mixture filtrate to evaporate slowly at room temperature. The infrared spectrum of the precipitate which formed during the reaction was identical with that of the single crystals. A crystal of irregular shape (0.17mm X 0.15mm X 0.05mm) was cut from the larger crystals and used for single crystal X-ray structure determination.The crystal density was measured by suspension in a solution of bromoform and methanol. The crystal was mounted on a glass pin for data collection. Unit cell parameters were refined by a least-squares fit of 23 reflections at 2θ angles between 14.5° and 29.3°. A psi-scan was made to correct for absorption problems, with the approximation that the crystal was lamellar. A $\theta,2\theta$ scan was used to obtain intensity data. The structure was solved by direct methods. The positions of the hydrogen atoms were determined by the neutron diffraction study (see Section 2.3). The hydrogen atom site occupancy factors were each fixed at 0.67. The oxygen-hydrogen bond lengths were refined against the X-ray data with the use of fixed isotropic temperature factors. The zinc atom was located on the two-fold axis and fixed in the x,y, and z directions (*i.e.* only the anisotropic temperature factors were refined). Scale, positional parameters, and the anisotropic temperature factors for the remaining atoms were varied to minimize the least squares function (Equation 2.1.3(f)). Further details regarding the specimen, the data collection and refinement are given in Table 2.2.2.

TABLE 2.2.2 Crystallographic Parameters for Bis(2,4,5-tribromoimidazole)diaquozinc(II)

Formula / Formula weight	$C_6H_4Br_6N_4O_2Zn$ / 708.96
Crystal colour / Shape / Size (mm)	colourless / irregular / 0.17 x 0.15 x 0.05
Space Group / Cell Setting	Aba2 / Orthorhombic
Incident Radiation (Å)	Ag K_α (0.56086)
Unit cell parameters (Å and degrees)	a = 1.4140(2) b = 15.348(3) c = 9.547(2)
	$\alpha = \beta = \gamma = 90.00$
Volume ($Å^3$) / Z	1676.3(6) / 4
ρ_{calc} / ρ_{obs} (Mg m^{-3})	2.809 / 2.77(1)
2θ Range (degrees)	$4.18 \leq 2\theta \leq 40.1$
Indices Range	$-1 \leq h \leq 13, -18 \leq k \leq 1, -11 \leq l \leq 11$
Temperature (°C)	22(1)
Absorption coefficient (mm^{-1})	8.424
Transmission factor range	0.657 - 1.000
Standards / Decay	3 standards checked every 97 measurements varied
	from 0.9847 to 1.0303
# of Reflns Measured / # of Unique Reflns	1875 / 1584
R_{int}	0.0328
F(000)	1296
# of Parameters for Refinement / # Restraints	87 / 1
R / R_w	0.0440 / 0.0715
Final $\Delta \sigma^{-1}$ -- Maximum / Average	0.004 / 0.000
Final Difference map -- Max / Min (e $Å^{-3}$)	0.520 / -0.451
Weighting	$w= [\sigma^2(F_o^2)+(0.0410P)^2]^{-1}$ $P=(F_o^2+2F_c^2)^3$
S	0.921

2.2.3 Catena di-μ-imidazolatozinc(II)

The crystal density was measured by suspension in carbon tetrachloride. The crystal was mounted on a glass pin for data collection. Unit cell parameters were refined by a least-squares fit of 33 reflections at 2θ angles between 14.72° and 29.60°. The (100), (-100), (110), (1-10), and the (-110) faces of the crystal were indexed and measured and used in a Gaussian absorption correction. An ω scan was used to obtain intensity data. The structure was solved by direct methods. Hydrogen atoms were placed in calculated positions with fixed isotropic temperature factors and not refined. Scale, positional parameters, and the anisotropic temperature factors were varied to minimize the least squares function (Equation 2.1.3(f)). Further details of the data collection and refinement are given in Table 2.2.3.

TABLE 2.2.3 Crystallographic Parameters for Catena di-μ-imidazolatozinc(II)

Formula / Formula weight	$C_{12}H_{12}N_8Zn_2$ / 399.04
Crystal colour / Shape / Size (mm)	colourless / needles / 0.14 x 0.10 x 0.09
Space Group / Cell Setting	$I4_1cd$ / tetragonal
Incident Radiation (Å)	Ag K_α (0.56086)
Unit cell parameters (Å and degrees)	a = 23.408(5) b = 23.412(5) c = 12.413(2)
	$\alpha = \beta = \gamma = 90.00$
Volume (Å^3) / Z	6802.7(23)/ 16
ρ_{calc} / ρ_{obs} (Mg m^{-3})	1.558 / 1.59(2)
2θ Range (degrees)	$3.88 \leq 2\theta \leq 40.08$
Indices Range	$0 \leq h \leq 28$, $0 \leq k \leq 28$, $-13 \leq l \leq 15$
Temperature (°C)	22(1)
Absorption coefficient (mm^{-1})	1.489
Transmission factor range	0.731-0.771
Standards / Decay	3 standards checked every 97 measurements varied from 0.9866 to 1.0210
# of Reflections Measured / # of Unique Reflections	5393 / 2752
R_{int}	0.0579
F(000)	3200
# of Parameters for Refinement / # Restraints	199 / 1
R / R_w	0.08 / 0.0584
Flack Parameter	-0.03(4)
Final $\Delta\sigma^{-1}$ -- Maximum / Average	0.00 / 0.04
Final Difference map -- Max / Min (e Å^{-3})	0.31 / -0.26
Weighting	$w = [\sigma^2(F_o^2)+(0.0138P)^2]^{-1}$ $P=(F_o^2+2F_c^2)^3$
S	0.810

Alpha OpenVMS system. This software incorporates programs taken from the public domain such as ortep, orfls, and orffe.

A radial scan was used for data collection. The radial scan was developed at Oak Ridge Laboratories. A $\theta/2\theta$ scan is along the diffraction vector, and an ω scan is perpendicular to the diffraction vector. A radial scan is along the radius of Ewald's sphere. As a result, the radial scan is equivalent to the ω scan at $2\theta=0^\circ$ and equivalent to the $\theta/2\theta$ scan at $2\theta=180^\circ$.

Three reflections [(020), (002), (-1-20)] were chosen as standards and monitored every 27 measurements. No appreciable decay of these standards was observed. Data was collected for $3.5^0 < 2\theta < 50^\circ$. After the data collection, a ψ-scan was used to correct for absorption.

The unit cell and its contents as obtained from single crystal X-ray analysis, with the exception of the atomic hydrogen positions, was used as a starting point for the least squares data refinement. The hydrogen positions were located by difference Fourier maps.

2.4 Vibrational Spectroscopy

Infrared spectra were recorded on a Bio Rad FTS-40 spectrometer. Solid samples were prepared as KBr pellets (1-5%). Spectra were calibrated against a polystyrene sample. The sample chamber was purged with dry nitrogen. The empty sample chamber was scanned to provide a background spectrum, which was subtracted from the sample spectrum. For both background and sample specta, a total of 16 scans at 2 cm^{-1} resolution were performed before applying a Fourier Transform to provide a spectrum. For sample spectra, baseline corrections were performed manually.

2.5 Elemental Analysis

Elemental analyses were performed by Guelph Chemical Laboratories in Guelph, Ontario, Canada.

2.6 Synthetic Procedures

All chemicals were from the Aldrich Chemical Company and the BDH Chemical Company and used without further purification.

2.6.1 Preparation of 2,4,5-tribromoimidazole (I)

2,4,5-tribromoimidazole (I) was prepared by the method of Wahren[44]. The melting point (212-216°C, decomposition) matched the literature value (213-215°C). Experimental results (infrared, pKa measurements) indicated that it was the acetate salt of the protonated form of 2,4,5-tribromoimidazole which was actually isolated from this preparation.

2.6.2 Preparation of bis(2,4,5-tribromoimidazole)diaquozinc(II) (II)

Compound (II) was formed by dissolving tribromoimidazole (0.28g, 0.9 mmol) in concentrated NH_4OH (20 ml). $Zn(NO_3)_2 \cdot 6H_20$ (0.091 g, 0.3 mmol) was added to the resulting solution. A colourless precipitate formed within 5 minutes which was isolated from the solution by filtration. The filtrate was allowed to stand for 2 weeks, which resulted in the formation of large transluscent yellow single crystals. The infrared spectrum of the colourless precipitate was identical to that of the single crystals. The yield was 80% (0.17 g, 0.24 mmol). The melting point of the single crystals was greater than 360°C. Elemental analysis: found (C 10.4%, H 0.8%, N 11.7%, Zn 7.7%, Br 67.5%) expected (C 10.2%, H 0.6%, N 7.9%, Zn 9.2%, Br 67.6%).

2.6.3 Preparation of deuterated form of bis(2,4,5-tribromoimidazole)diaquozinc(II) (II-D)

The preparation of (**II-D**) was the same as for (**II**) (given in 2.6.2), except that concentrated ND_4OD was used in place of concentrated NH_4OH. An IR spectrum of the colourless precipitate was taken for comparison with the non-deuterated sample. No single crystals were obtained. The powder X-ray diffraction pattern (Section 3.3.3) was identical to that of the non-deuterated sample.

2.6.4 Preparation of Catena di-μ-imidazolatozinc(II) (III)

The synthesis of (**III**) was similar to the synthesis of (**II**) except that imidazole was used instead of tribromoimidazole. Imidazole (6.84 g, 10.1 mmol) was dissolved in concentrated NH_4OH. $Zn(NO_3)_2{\cdot}6H_20$ (2 g, 6.7 mmol) was added to the resulting solution. A colourless precipitate formed within five minutes and was isolated from the solution by filtration. Colourless, transparent, needle-shaped single crystals precipitated from the filtrate within two days. The melting point was greater than 360° C. The infrared spectra of the colourless precipitate and single crystals matched exactly. The yield was 90% (1.2g, 6 mmol) Elemental analysis: found (C 35.7%, H 3.1%, N 28.1%) expected (C 35.9%, H 3.0%, N 28.0%).

2.6.5 Preparation of bis(2,4,5-tribromoimidazole)diaquocopper(II) (IV)

Compound (IV) was prepared in a manner similar to (II) except that copper nitrate was used in place of zinc nitrate. Tribromoimidazole (1.5 g, 4.9 mmol) was dissolved in 30 ml of concentrated NH_4OH. Cupric nitrate (0.40 g, 1.6 mmol) was added to the resulting solution. The solution went from blue to colourless as dark red crystals precipitated. The crystals were birefringent, displaying either a dark red or a dark green colour when viewed under the microscope. The crystals were able to extinguish plane polarized light but were unsuitable for X-ray diffraction. The infrared spectrum of the product was similar to the infrared spectrum of (II) (comparison is shown in Section 3.5). The yield was 75% (0.85 g, 1.2 mmol). The melting point of the crystals was 140°C -143°C with decomposition. Elemental analysis: found (C 10.0%, H 0.8%, N 11.6%, Cu 6.4%, Br 69.5%) expected (C 10.2%, H 0.6%, N 7.9%, Cu 9.0%, Br 67.8%).

2.7 Titration Data

The titration of $ImBr_3$ (I) was performed with a Tanager Scientific Systems 8901 autotitrator. The sample was stirred and purged with nitrogen during the measurement. A background sample was run to correct for any carbonate which may have been present in the system. A 0.1 M KCl solution was added to all solutions to level the background electrolyte concentration.

The pKa value was determined from the inflection point in a plot of pH versus time on the titrator (see Figure 3.2(a)). The error was derived from the width of the peak in the plot of the rate of change of the pH with respect to the time versus time (see Figure 3.2(b)). The pKa value for (**I**) was determined to be 10.7(2). The second pKa value could not be obtained because the diprotonated molecule was insoluble in water.

2.8 Molecular Orbital Calculations

Molecular orbital calculations on (**II**) were performed with CACAO software package[45]. The Z-matrix reference system was used to define the molecular geometry. The results from the Z-matrix file were compared against a similar file defined solely by crystallographic coordinates. The comparison was exact, meaning that the Z-matrix file defined a molecule with the same geometry found in the crystal structure of (**II**).

3. RESULTS

3.1 Triaquo(tris-2-pyridylphosphine)nickel(II) dinitrate

A diagram of the molecular geometry is shown in Figure 3.1(a). The molecular packing is shown in Figure 3.1(b). Positional and thermal parameters are quoted for all atoms (except calculated hydrogen atom positions) in Table 3.1(a). Bond lengths and angles are quoted for only 1 of the molecules of triaquo(tris-2-pyridylphosphine)nickel(II) dinitrate in the asymmetric unit in Tables 3.1(b-c).

Figure 3.1(a) Molecular geometry of Triaquo(tris-2-pyridylphosphine)nickel(II)

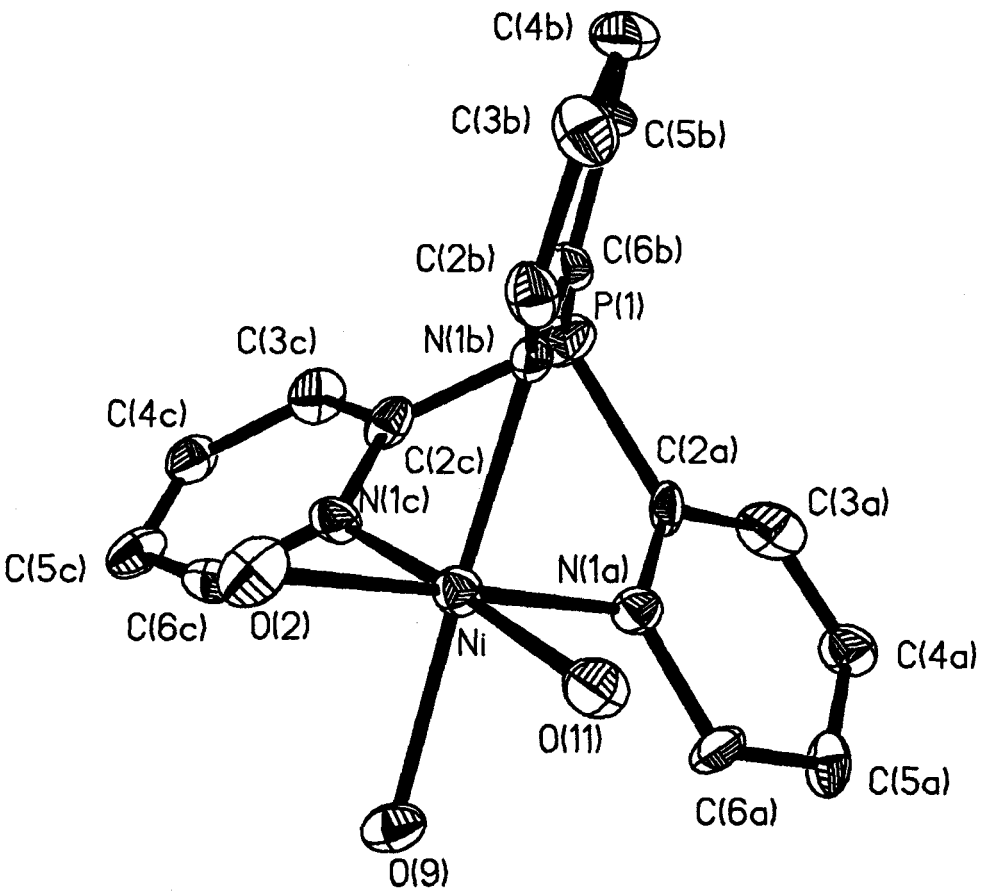

Thermal ellipsoids are shown at the 30% probability level. Hydrogen atoms, water of crystallization, counterions, and one of the molecules in the asymmetric unit have been omitted for clarity.

Figure 3.1(b) Molecular packing in Triaquo(tris-2-pyridylphosphine)nickel(II) dinitrate

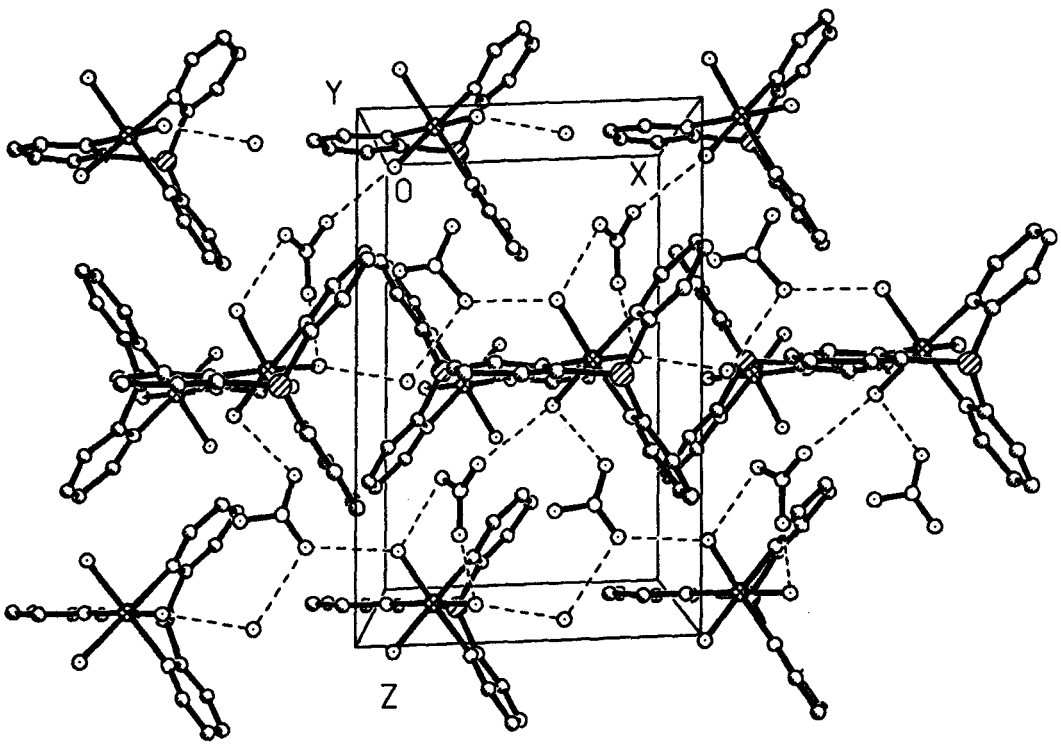

As viewed down the [010] axis. Hydrogen bonding interactions are indicated with dashed lines. Hydrogen atoms have been omitted for clarity. The carbon atoms are shown as shaded circles, the oxygen atoms as circles containing dots, the nitrogen atoms as open circles, the nickel atoms as circles containing an X, and the phosphorus atoms as circles with slanted lines.

Table 3.1(a) Positional and Equivalent Isotropic Thermal Parameters of Triaquo(tris-2-pyridylphosphine)nickel(II) dinitrate

Atom	x	y	z	U_{eq}
Ni	0.2971(2)	0.26549(7)	0.5219(1)	0.0312(5)
P1	0.2267(6)	0.4620(3)	0.4903(3)	0.048(1)
O2	0.404(1)	0.2160(6)	0.6402(7)	0.045(3)
N1A	0.183(2)	0.3151(8)	0.4070(8)	0.033(3)
O9	0.155(1)	0.1679(6)	0.5269(7)	0.039(3)
O11	0.422(1)	0.1891(7)	0.4344(8)	0.044(3)
N1C	0.170(2)	0.3339(7)	0.6093(9)	0.036(3)
C5A	0.034(2)	0.2944(1)	0.259(1)	0.042(4)
C6A	0.120(2)	0.2629(9)	0.338(1)	0.038(4)
N1B	0.454(1)	0.3546(8)	0.5116(8)	0.032(3)
C4A	0.008(2)	0.377(1)	0.253(1)	0.045(4)
C2A	0.157(2)	0.3921(9)	0.3989(8)	0.033(4)
C6B	0.599(2)	0.3344(9)	0.521(1)	0.038(4)
C2B	0.415(2)	0.4335(8)	0.501(1)	0.035(3)
C4C	-0.022(2)	0.419(1)	0.724(1)	0.048(4)
C5C	-0.006(2)	0.3440(1)	0.7404(1)	0.044(4)
C2C	0.145(2)	0.413(1)	0.592(1)	0.035(4)
C3B	0.519(2)	0.490(1)	0.499(1)	0.039(3)
C3C	0.047(2)	0.4562(9)	0.648(1)	0.045(4)
C4B	0.681(2)	0.467(1)	0.504(1)	0.056(5)
C6C	0.094(2)	0.3049(8)	0.680(1)	0.039(3)
C5B	0.715(2)	0.386(1)	0.514(1)	0.048(4)
C3A	0.077(2)	0.4210(9)	0.323(1)	0.053(4)
O5	0.205(2)	0.0618(8)	0.6788(8)	0.052(3)
Ni1	0.2031(2)	0.51672(7)	0.9784(1)	0.0298(5)
P3	0.2732(6)	0.3202(3)	1.0118(3)	0.040(1)
O3	0.090(1)	0.5679(6)	0.8606(6)	0.042(3)
O4	0.341(1)	0.6130(6)	0.9714(7)	0.038(3)
O6	0.080(1)	0.5935(7)	1.0664(7)	0.040(3)
N10	0.325(2)	0.4692(8)	1.0954(8)	0.034(3)
N15	0.333(2)	0.4449(8)	0.8886(8)	0.035(3)
C19	0.382(2)	0.5125(8)	1.159(1)	0.035(3)
H19A	0.369(2)	0.5690(8)	1.152(1)	0.08
N24	0.039(2)	0.4314(7)	0.9865(9)	0.040(3)
C31	0.526(2)	0.3556(9)	0.786(1)	0.053(4)
H31A	0.598(2)	0.3257(9)	0.752(1)	0.08
C34	0.074(2)	0.355(1)	0.997(1)	0.038(3)

Table 3.1(a) Positional and Equivalent Isotropic Thermal Parameters of Triaquo(tris-2-pyridylphosphine)nickel(II) dinitrate (continued)

Atom	x	y	z	U_{eq}
C37	0.495(2)	0.440(1)	0.763(1)	0.051(5)
H37A	0.545(2)	0.465(1)	0.712(1)	0.08
C38	0.345(2)	0.388(9)	1.107(1)	0.038(4)
C44	-0.104(2)	0.452(1)	0.984(1)	0.041(4)
H44A	-0.133(2)	0.507(1)	0.981(1)	0.08
C46	-0.042(2)	0.2963(1)	1.004(1)	0.046(4)
H46A	-0.015(2)	0.241(1)	1.013(1)	0.08
C47	0.358(2)	0.368(1)	0.908(1)	0.038(4)
C48	-0.213(2)	0.392(1)	0.986(1)	0.056(5)
H48A	-0.316(2)	0.406(1)	0.981(1)	0.08
C49	0.448(2)	0.321(1)	0.857(1)	0.044(4)
H49A	0.455(2)	0.265(1)	0.869(1)	0.08
C53	0.398(2)	0.482(1)	0.8144(9)	0.043(4)
H53A	0.375(2)	0.536(1)	0.7989(9)	0.08
C55	0.430(2)	0.3544(9)	1.1805(8)	0.038(3)
H55A	0.447(2)	0.2980(9)	1.1870(8)	0.08
C62	0.463(2)	0.4890(9)	1.236(1)	0.046(4)
H62A	0.501(2)	0.5260(9)	1.2836(1)	0.08
C63	-0.176(2)	0.315(1)	0.994(1)	0.057(6)
H63A	-0.251(2)	0.274(1)	0.993(1)	0.08
C71	0.485(2)	0.412(1)	1.248(1)	0.053(5)
H71A	0.545(2)	0.394(1)	1.302(1)	0.08
H2A	0.469(1)	0.1794(6)	0.6336(7)	0.08
H2B	0.384(1)	0.2322(6)	0.6961(7)	0.08
H5AA	-0.008(2)	0.258(1)	0.211(1)	0.08
H6AA	0.136(2)	0.2064(9)	0.344(1)	0.08
H4AA	-0.050(2)	0.401(1)	0.201(1)	0.08
H6BA	0.622(2)	0.2795(9)	0.534(1)	0.08
H4CA	-0.083(2)	0.450(1)	0.766(1)	0.08
H5CA	-0.058(2)	0.317(1)	0.790(1)	0.08
H3BA	0.492(2)	0.546(1)	0.493(1)	0.08
H3CA	0.026(2)	0.5112(9)	0.634(1)	0.08
H4BA	0.758(2)	0.506(1)	0.501(1)	0.08
H6CA	0.110(2)	0.2492(8)	0.693(1)	0.08
H5BA	0.816(2)	0.367(1)	0.515(1)	0.08

Table 3.1(a) Positional and Equivalent Isotropic Thermal Parameters of Triaquo(tris-2-pyridylphosphine)nickel(II) dinitrate (continued)

Atom	x	y	z	U_{eq}
N13	0.207(1)	0.0799(6)	0.7644(6)	0.036(3)
O17	0.150(1)	0.0387(7)	0.8258(8)	0.051(3)
O27	0.264(2)	0.1425(8)	0.7954(9)	0.066(4)
N16	0.295(1)	0.7053(7)	0.7334(8)	0.053(3)
O18	0.296(1)	0.7218(8)	0.8205(8)	0.054(4)
O26	0.349(1)	0.7542(7)	0.6781(8)	0.053(3)
O35	0.233(1)	0.6403(8)	0.7098(9)	0.056(3)
O22	0.407(1)	0.1436(9)	0.217(1)	0.075(4)
N33	0.279(2)	0.1151(7)	0.2243(9)	0.045(4)
O41	0.2021(1)	0.104(1)	0.1545(8)	0.107(6)
O56	0.246(1)	0.0889(7)	0.3029(9)	0.054(3)
O43	0.271(2)	0.6946(9)	0.203(1)	0.086(5)
N45	0.214(2)	0.6692(9)	0.278(1)	0.065(4)
O61	0.098(1)	0.6387(9)	0.2855(9)	0.068(4)
O60	0.309(2)	0.6649(9)	0.3530(9)	0.076(3)
O1W	0.629(1)	0.596(1)	1.0120(9)	0.065(4)
O2W	-0.126(2)	0.189(1)	0.4903(9)	0.079(5)

Table 3.1(b) Selected Bond Lengths for Triaquo(tris-2-pyridylphosphine)nickel(II) dinitrate

Atoms	*Bond Length (Å)*	*Bond Length (Å)**	*Atoms*	*Bond Length (Å)*	*Bond Length (Å)**
Ni-N1C	2.05(1)	2.11(1)	N1B-C6B	1.34(2)	1.33(2)
Ni-N1A	2.05(1)	2.09(1)	N1B-C2B	1.37(2)	1.32(2)
Ni-N1B	2.06(1)	2.06(1)	C4A-C3A	1.35(2)	1.42(2)
Ni-O9	2.08(1)	2.04(1)	C2A-C3A	1.34(2)	1.38(2)
Ni-O2	2.06(1)	2.09(1)	C6B-C5B	1.36(2)	1.40(2)
Ni-O11	2.11(1)	2.11(1)	C2B-C3B	1.34(2)	1.44(2)
P1-C2B	1.76(2)	1.89(2)	C4C-C5C	1.28(2)	1.47(2)
P1-C2C	1.82(2)	1.84(2)	C4C-C3C	1.39(2)	1.36(2)
P1-C2A	1.82(2)	1.84(2)	C5C-C6C	1.41(2)	1.35(2)
N1A-C2A	1.32(2)	1.38(2)	C2C-C3C	1.40(2)	1.35(2)
N1A-C6A	1.41(2)	1.25(2)	C3B-C4B	1.50(3)	1.25(3)
N1C-C6C	1.31(2)	1.35(2)	C4B-C5B	1.40(3)	1.33(3)
N1C-C2C	1.36(2)	1.33(2)	C5A-C4A	1.41(2)	1.32(2)
			C5A-C6A	1.42(2)	1.33(2)

*The second bond length listings are for the equivalent atoms in the second molecule in the unit cell.

Table 3.1(c) Selected Bond Angles for Triaquo(tris-2-pyridylphosphine)nickel(II) dinitrate

Atoms	*Bond Angle (°)*	*Bond Angle (°)*†	*Atoms*	*Bond Angle (°)*	*Bond Angle (°)*
N1C-Ni-N1A	87.9(5)	87.7(5)	C2C-N1C-Ni	122(1)	121(1)
N1C-Ni-N1B	91.8(5)	92.7(5)	C4A-C5A-C6A	112(2)	118(2)
N1A-Ni-N1B	88.7(5)	92.9(5)	N1A-C6A-C5A	120(1)	127(1)
N1C-Ni-O9	93.8(5)	94.2(5)	C6B-N1B-C2B	120(1)	121(1)
N1A-Ni-O9	93.1(5)	92.1(5)	C6B-N1B-Ni	118(1)	119(1)
N1B-Ni-O9	174.2(5)	171.6(5)	C2B-N1B-Ni	122(1)	120(1)
N1C-Ni-O2	90.3(5)	91.9(5)	C3A-C4A-C5A	115(2)	112(2)
N1A-Ni-O2	177.8(5)	177.3(5)	N1A-C2A-C3A	121(2)	119(1)
N1B-Ni-O2	92.5(4)	89.8(5)	N1A-C2A-P1	121(1)	122(1)
O9-Ni-O2	85.8(4)	85.3(4)	C3A-C2A-P1	119(2)	124(1)
N1C-Ni-O11	176.8(5)	177.2(5)	N1B-C6B-C5B	125(2)	119(2)
N1A-Ni-O11	93.2(5)	92.9(5)	C3B-C2B-N1B	121(2)	121(2)
N1B-Ni-O11	91.2(5)	90.0(5)	C3B-C2B-P1	118(1)	118(1)
O9-Ni-O11	83.1(4)	83.0(4)	N1B-C2B-P1	121(1)	121(1)
O2-Ni-O11	88.5(4)	87.3(4)	C5C-C4C-C3C	122(1)	118(1)
C2B-P1-C2C	102.9(7)	101.2(8)	C4C-C5C-C6C	115(2)	120(2)
C2B-P1-C2A	101.1(7)	101.0(7)	N1C-C2C-C3C	121(2)	124(2)
C2C-P1-C2A	96.6(7)	98.7(7)	N1C-C2C-P1	121(1)	121(1)
C2A-N1A-C6A	119(1)	116(1)	C3C-C2C-P1	118(1)	116(1)
C2A-N1A-Ni	123(1)	122(1)	C2B-C3B-C4B	119(2)	121(2)
C6A-N1A-Ni	118(1)	122(1)	C4C-C3C-C2C	119(1)	118(2)
C6C-N1C-C2C	114(1)	122(1)	C5B-C4B-C3B	118(2)	119(2)
C6C-N1C-Ni	124(1)	117(1)	N1C-C6C-C5C	129(2)	118(2)
C2A-C3A-C4A	126(2)	113(1)	C6B-C5B-C4B	117(2)	122(2)

3.2 pKa Measurement for (I)

The pKa measurement for **(I)** was accomplished as indicated in Section 2.7. The autotitrator added variable amounts of 0.1 M HCl at regular intervals in order to obtain a good resolution for the pH measurements in areas where the pH was changing rapidly. It was therefore prudent to use the plot of pH versus time (shown below in Figure 3.2(a) to find the inflection points on the graph which would, in turn, give the pKa values for **(I)**. The data was treated with the Tanager package[46] which allows the subtraction of a

†The second bond angle listings are for the equivalent atoms in the second molecule in the unit cell.

background run from the sample run, thereby eliminating interferences such as dissolved CO_2. The sharp break in the titration curve at the 0.7 hour mark is caused by the precipitation of the doubly protonated species. A ratio of pH change to time change was calculated for each point and plotted against time (see Figure 3.2(b)). This helped to identify the place of sharpest inflection on the titration curve, and thus the second pKa value for **(I)**.

FIGURE 3.2(a) Plot of pH Versus Time for Titration Of 2,4,5-Tribromoimidazole with 0.1 M HCl

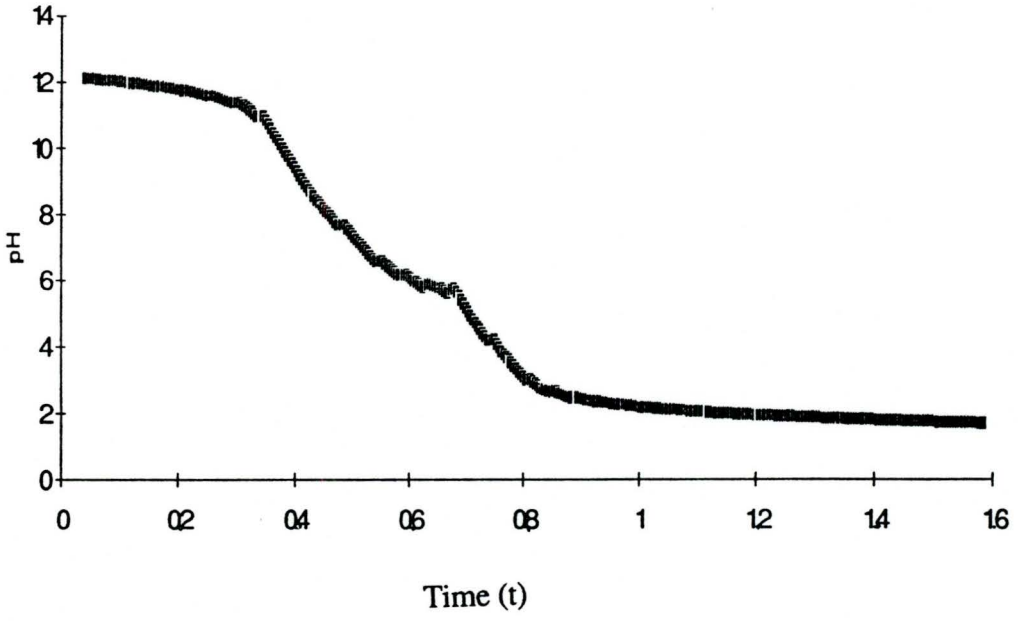

FIGURE 3.2(b) Plot of Change in pH / Change in Time Versus Time

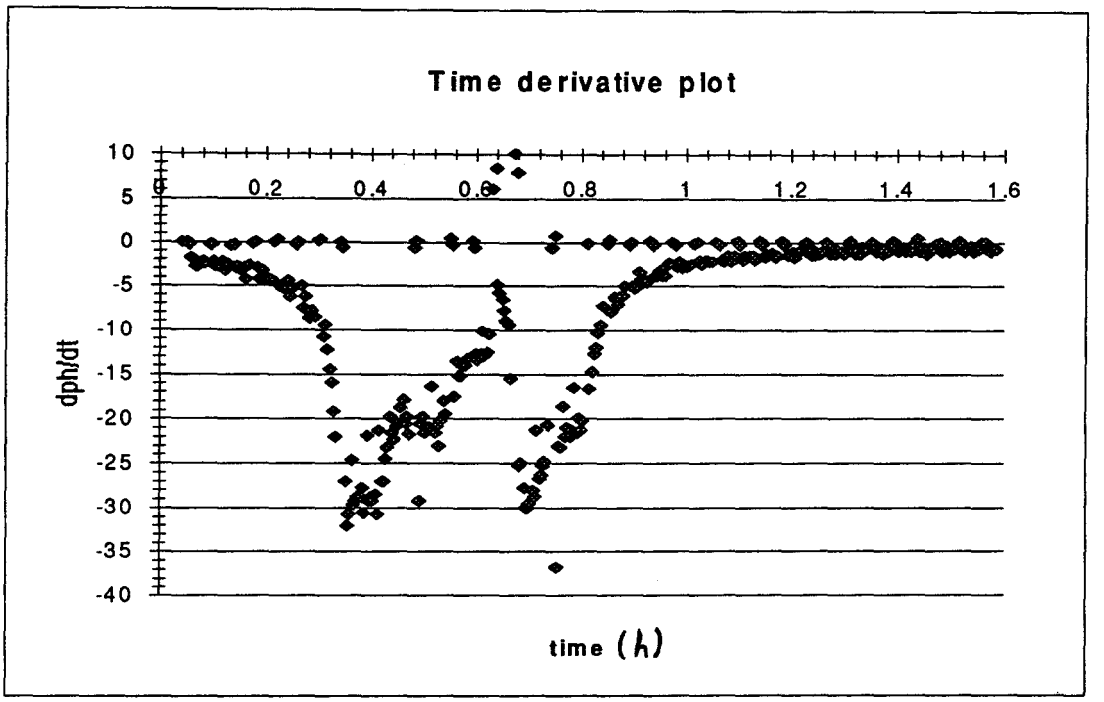

3.3 *Bis(2,4,5-tribromoimidazole)(diaquo)zinc(II) (II)*

3.3.1 X-Ray Results

The ligands bind in a tetrahedral fashion to the zinc atom. The zinc nitrogen and zinc oxygen bond lengths are not unusual. The atoms in the tribromoimidazole rings are all planar with the exception of the bromine atoms which are slightly above the plane of the ring atoms. The tribromoimidazole rings pack such that they form approximately 90° angles to each other within the lattice when viewed down the [001] axis. The molecules pack in parallel planes along the [001] axis, with the planes being held together by hydrogen bonding interactions. Atomic positions and equivalent isotropic temperature factors are given in Table 3.3.1(a). Bond lengths are shown in Table 3.3.1(b), torsion

angles are presented in Table 3.3.1(c) and bond angles can be found in Table 3.3.1(d). The molecular geometry with all hydrogen positions is shown in Figure 3.3.1(a). Two different packing diagrams are shown: Figure 3.3.1(b) shows packing with all intermolecular hydrogen bonding, while Figure 3.3.1(c) illustrates the packing of the ring atoms. The structure of (**II**) is discussed further in Section 4.2.

TABLE 3.3.1(a) Atomic Coordinates, Equivalent Isotropic Temperature Factors, And Site Occupancies For $Zn(ImBr_3)_2(OH_2)_2$

	x	*y*	*z*	*U(eq)*[§]	*Occ.*
Zn1	0	0	0.7010(1)	0.0327(3)	1
O1	0.0412(6)	0.0971(4)	0.8444(6)	0.062(2)	1
N1	-0.1280(5)	0.0476(4)	0.5881(7)	0.034(2)	1
C2	-0.2417(6)	0.0287(5)	0.5715(8)	0.033(2)	1
N3	-0.2982(5)	0.0745(4)	0.4769(7)	0.035(2)	1
C4	-0.2137(7)	0.1291(5)	0.4300(8)	0.036(2)	1
C5	-0.1130(7)	0.1127(5)	0.4925(8)	0.031(2)	1
Br2	-0.31635(7)	-0.05650(6)	0.6796(1)	0.0523(3)	1
Br4	-0.24367(8)	0.21351(5)	0.2918(1)	0.0471(2)	1
Br5	0.03131(7)	0.17002(6)	0.4718(1)	0.0507(2)	1
H1B	0.084	0.1589	0.8223	0.076[**]	0.67[††]
H1A	0.0538	0.058	0.962	0.076	0.67
H1C	-0.0421	0.1296	0.9012	0.076	0.66

TABLE 3.3.1(b) Bond Lengths For $Zn(ImBr_3)_2(OH_2)_2$

Atoms	*Length (Å)*
Zn1-N1	2.008(6)
Zn1-O1	2.022(6)
O1-H1B	1.088(6)
O1-H1A	1.281(6)
O1-H1C	1.205(7)
N1-C2	1.341(9)
N1-C5	1.364(9)
C2-N3	1.32(1)
C2-Br2	1.872(7)
N3-C4	1.36(1)
C4-C5	1.32(1)
C4-Br4	1.881(8)
C5-Br5	1.881(7)

[§] The equivalent isotropic U is defined as one third of the trace of the orthogonalized U_{ij} tensor.
[**] Temperature factors for hydrogen atoms were anisotropic and were not refined.
[††] Occupancy factors for hydrogen were determined from single crystal neutron diffraction.

TABLE 3.3.1(c) TORSION ANGLES FOR $Zn(ImBr_3)_2(OH_2)_2$

Atoms	*Angle (°)*
N1-Zn1-N1-C2	119.2(8)
O1-Zn1-N1-C2	-113.2(7)
O1-Zn1-N1-C2	-1.2(8)
N1-Zn1-N1-C5	-59.4(5)
O1-Zn1-N1-C5	68.2(6)
O1-Zn1-N1-C5	-179.7(5)
C5-N1-C2-N3	0.1(9)
Zn1-N1-C2-N3	-178.7(6)
C5-N1-C2-Br2	-178.8(5)
Zn1-N1-C2-Br2	2(1)
N1-C2-N3-C4	-1.2(9)
Br2-C2-N3-C4	177.6(5)
C2-N3-C4-C5	2.0(9)
C2-N3-C4-Br4	-179.0(6)
N3-C4-C5-N1	-2.1(10)
Br4-C4-C5-N1	179.0(6)
N3-C4-C5-Br5	-178.1(6)
Br4-C4-C5-Br5	3(1)
C2-N1-C5-C4	1.2(9)
Zn1-N1-C5-C4	-179.8(5)
C2-N1-C5-Br5	177.5(5)
Zn1-N1-C5-Br5	-3.5(9)

TABLE 3.3.1(d) BOND ANGLES FOR $Zn(ImBr_3)_2(OH_2)_2$

Atoms	*Angle (°)*
N1-Zn1-N1	109.2(4)
N1-Zn1-O1	105.6(3)
N1-Zn1-O1	117.8(3)
O1-Zn1-O1	101.2(4)
Zn1-O1-H1B	128.6(4)
Zn1-O1-H1A	103.7(4)
H1B-O1-H1A	121.8(5)
Zn1-O1-H1C	114.0(4)
H1B-O1-H1C	94.7(5)
H1A-O1-H1C	83.6(4)
C2-N1-C5	101.6(6)
C2-N1-Zn1	134.1(5)
C5-N1-Zn1	124.2(5)
N3-C2-N1	116.3(7)
N3-C2-Br2	121.8(5)
N1-C2-Br2	121.9(5)
C2-N3-C4	101.9(6)
C5-C4-N3	110.8(7)
C5-C4-Br4	127.3(6)
N3-C4-Br4	121.8(6)
C4-C5-N1	109.4(6)
C4-C5-Br5	129.0(6)
N1-C5-Br5	121.5(6)

FIGURE 3.3.1(a) Geometry of $Zn(ImBr_3)_2(OH_2)_2$. Thermal ellipsoids are shown at 50% Probability Level.

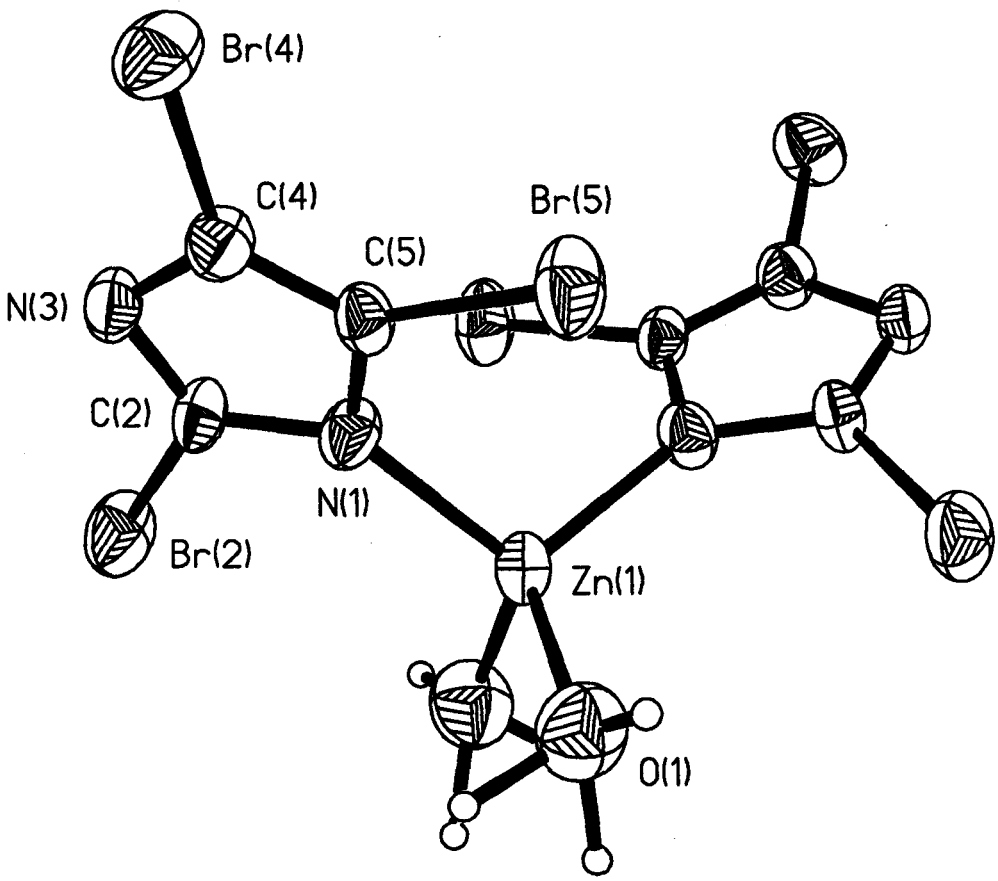

FIGURE 3.3.1(b) Molecular Packing in $Zn(ImBr_3)_2(OH_2)_2$ as Viewed Down [001] Axis

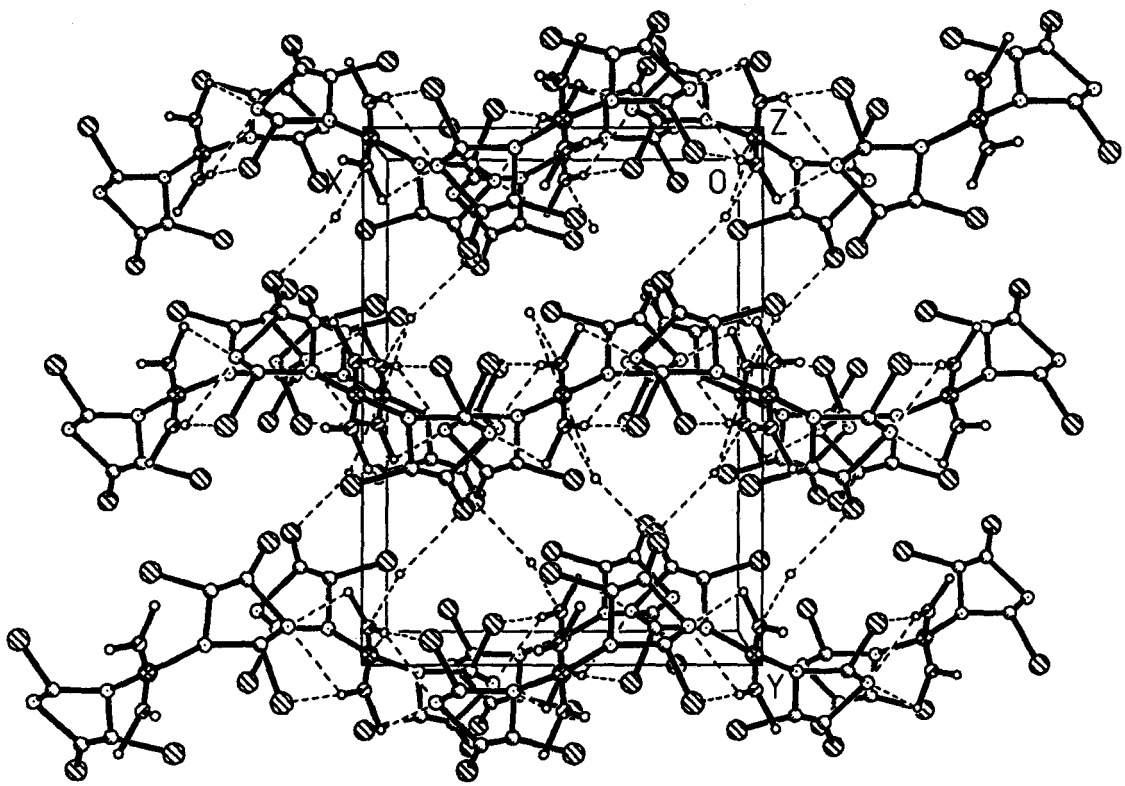

Intermolecular hydrogen bonding interactions are indicated with dashed lines. The bromine atoms are depicted as shaded circles, carbon atoms are open circles, nitrogen atoms are indicated by circles containing a dot, and zinc atoms are indicated by circles containing an X.

FIGURE 3.3.1(c) Molecular Packing in $Zn(ImBr_3)_2(OH_2)_2$ as Viewed Down [100] Axis

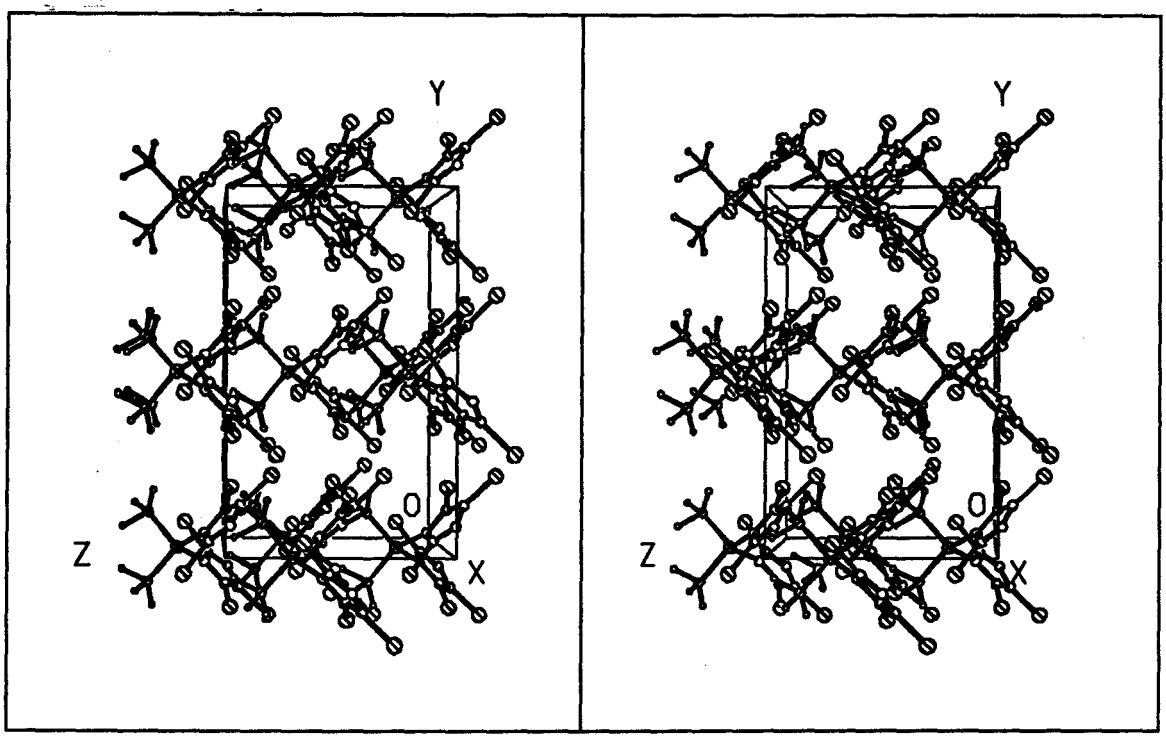

Nitrogen atoms are shown as circles containing a dot. Bromine atoms are indicated as circles containing slashes slanted to the left, oxygen atoms as circles with slashes slanted to the right. Zinc atoms are shown as circles containing an X and hydrogen atoms are shown as open circles.

3.3.2 Neutron Results

The single crystal neutron data was used only for the location of the hydrogen atoms. Therefore, only data concerning the hydrogen atoms is presented here. The bond lengths are shown in Table 3.3.2(a), the bond angles in Table 3.3.2(b). The atomic positions are given in Table 3.3.2(c).

TABLE 3.3.2(a)
Bond Lengths Involving Hydrogen Atoms for
$Zn(ImBr_3)_2(OH_2)_2$ from Neutron Diffraction Data.

Atoms	*Distance (Å)*
O(1)-H(1)	1.09(5)
O(1)-H(2)	1.11(5)
O(1)-H(3)	1.18(5)
N(3)-H(3)	2.01(4)
H(1)-H(2)	1.66(7)
H(1)-H(3)	1.83(6)
H(2)-H(3)	1.82(7)
O(1)-H(1)	1.09(5)
O(1)-H(2)	1.11(5)
O(1)-H(3)	1.18(5)
N(3)-H(3)	2.01(4)
H(1)-H(2)	1.66(7)
H(1)-H(3)	1.83(6)
H(2)-H(3)	1.82(7)

TABLE 3.3.2(b)
Angles Involving Hydrogen for
$Zn(ImBr_3)_2(OH_2)_2$ from Neutron Diffraction Data.

Atoms	*Angle (°)*
H(1)-O(1)-H(2)	98(4)
H(1)-O(1)-H(3)	108(3)
H(1)-O(1)-ZN(1)	119(3)
H(2)-O(1)-H(3)	105(3)
H(2)-O(1)-ZN(1)	118(3)
H(3)-O(1)-ZN(1)	108(2)
C(2)-N(3)-H(3)	139(2)
C(4)-N(3)-H(3)	116(1)
H(3)-N(3)-C(5)	150(1)
H(3)-N(3)-N(1)	167(2)
O(1)-H(1)-H(2)	41(3)
H(2)-H(1)-H(3)	63(3)
O(1)-H(2)-H(1)	41(2)
H(1)-H(2)-H(3)	63(3)
O(1)-H(3)-N(3)	148(3)
H(2)-H(3)-H(1)	54(3)
H(2)-H(3)-N(3)	146(3)
H(1)-H(3)-N(3)	158(3)

TABLE 3.3.2(c) Atomic Coordinates for $Zn(ImBr_3)_2(OH_2)_2$ from Neutron Diffraction Data

Atom	*x*	*y*	*z*
ZN(1)[‡‡]	0.0000	0.0000	0.0000
O(1)	0.0414(8)	0.0967(6)	0.133(3)
N(1)	-0.1267(7)	0.0479(6)	-0.124(3)
N(3)	-0.2981(8)	0.0756(6)	-0.234(3)
C(2)	-0.241(1)	0.0287(9)	-0.137(3)
C(4)	-0.214(1)	0.130(1)	-0.283(3)
C(5)	-0.112(1)	0.1134(8)	-0.213(3)
BR(2)	-0.317(1)	-0.056(1)	-0.031(4)
BR(4)	-0.240(2)	0.2148(9)	-0.417(3)
BR(5)	0.031(1)	0.170(1)	-0.236(4)
H(1)	0.122(4)	0.092(3)	0.194(6)
H(2)	0.057(4)	0.163(3)	0.089(6)
H(3)	-0.037(4)	0.106(2)	0.212(6)

[‡‡] The zinc atom was fixed at the origin.

Figure 3.3.3 X-Ray Powder Diffraction Data For $Zn(ImBr_3)_2(OH_2)_2$ and $Zn(ImBr_3)_2(OD_2)_2$

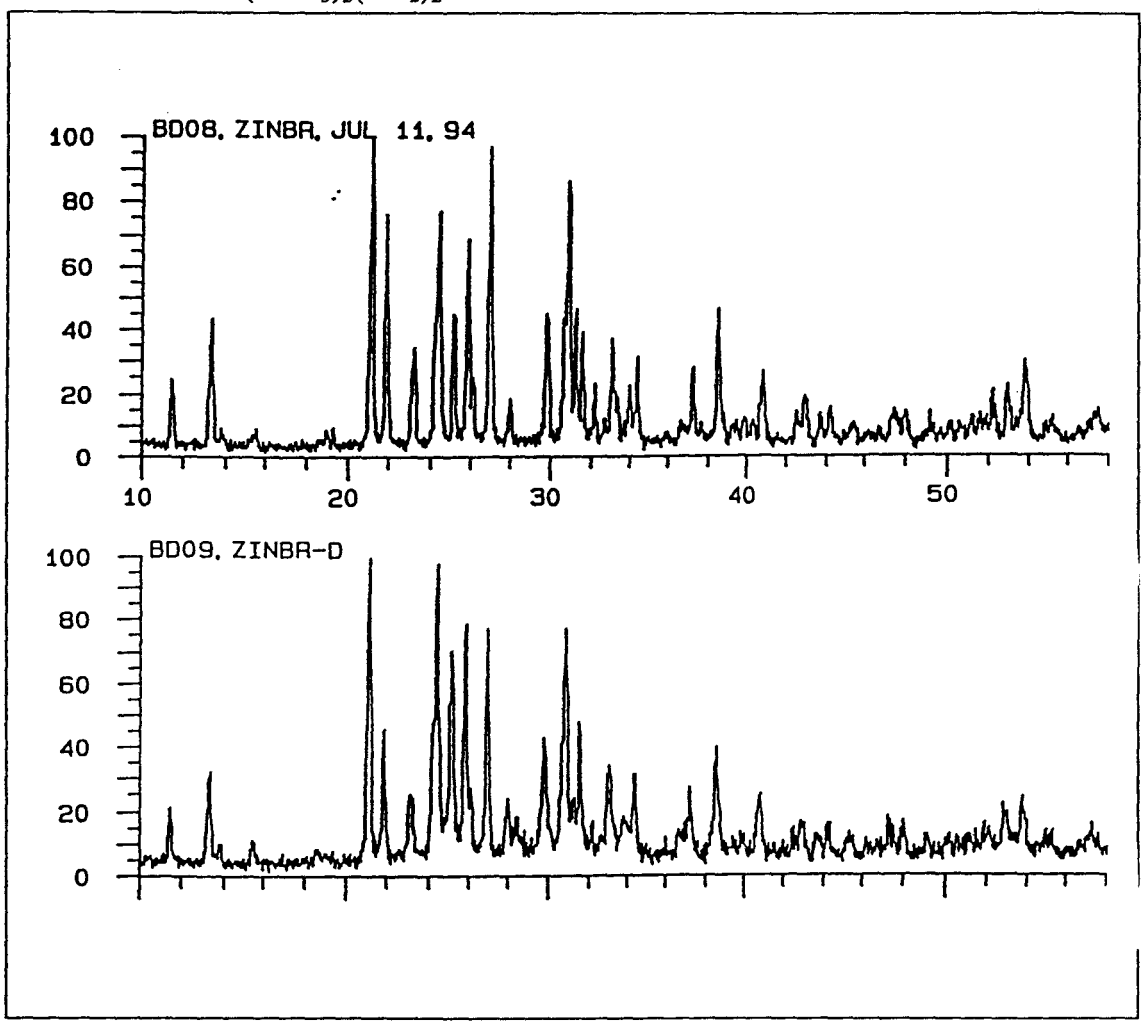

The x-axis shows the 2θ angle in degrees. The y-axis shows the normalized intensity. Molybdenum K_α radiation was used. The top diffraction pattern is from $Zn(ImBr_3)_2(OH_2)_2$ and the bottom diffraction pattern is from $Zn(ImBr_3)_2(OD_2)_2$.

3.4 Catena di-μ-imidazolatozinc (II)

3.4.1 Single Crystal X-Ray Results

Compound (III) forms a multiply catenated species in which both of the imidazole groups are bridging between zinc atoms. The result is a solid state structure with no discrete molecules. The coordination sphere around the zinc atom is approximately tetrahedral. There are two crystallographically different zinc atoms and four crystallographically different imidazole rings in the asymmetric unit. All of the rings are planar. Atomic positions and equivalent isotropic temperature factors are given in Table 3.4.1(a). Bond lengths are shown in Table 3.4.1(b), bond angles in Table 3.4.1(c). The assymetric unit is shown in Figure 3.4.1(a). Two different views of the packing are shown: Figure 3.4.1(b) demonstrates the packing of all atoms (except hydrogen) within the unit cell, while Figure 3.4.1(c) shows only the zinc and nitrogen atoms, demonstrating the tetrahedral coordination of the zinc by nitrogen.

TABLE 3.4.1(a) Atomic Coordinates and Equivalent Isotropic Temperature Factors for $Zn(Im)_2$

Atom	x	y	z	U(eq)
Zn1	0.60086(4)	0.35019(5)	0.94304(4)	0.0413(4)
Zn2	0.59621(4)	0.14822(5)	0.64796(5)	0.0414(4)
N1C	0.5147(3)	0.1511(3)	0.6163(8)	0.039(2)
N1A	0.5179(3)	0.3589(4)	0.9735(8)	0.053(3)
N3B	0.6236(3)	0.2819(3)	0.8600(6)	0.034(2)
C2B	0.5943(3)	0.2518(6)	0.789(1)	0.042(2)
H2BA	0.5577(3)	0.2616(6)	0.767(1)	0.05
N1B	0.6219(3)	0.2064(3)	0.7521(6)	0.039(2)
C2C	0.4736(4)	0.1202(4)	0.6639(9)	0.049(3)
H2CA	0.4811(4)	0.0946(4)	0.7195(9)	0.059
C2A	0.4761(4)	0.3767(4)	0.915(1)	0.055(3)
H2AA	0.4806(4)	0.3844(4)	0.842(1)	0.067
C5C	0.4850(4)	0.1789(4)	0.5400(8)	0.051(3)
H5CA	0.5011(4)	0.2047(4)	0.4919(8)	0.061
C5B	0.6741(3)	0.2095(3)	0.8006(6)	0.046(2)
H5BA	0.7043(3)	0.1843(3)	0.7903(6)	0.056
C4A	0.4368(5)	0.3643(5)	1.063(1)	0.099(5)
H4AA	0.4098(5)	0.3609(5)	1.118(1)	0.119
C4C	0.4306(4)	0.1656(4)	0.5413(8)	0.052(3)
H4CA	0.4031(4)	0.1787(4)	0.4933(8)	0.063
C4B	0.6744(3)	0.2552(3)	0.8656(6)	0.046(2)
H4BA	0.7050(3)	0.2666(3)	0.9082(6)	0.055
C5A	0.4938(5)	0.3505(5)	1.0713(9)	0.091(4)
H5AA	0.5124(5)	0.3378(5)	1.1330(9)	0.11
N3A	0.4266(4)	0.3835(3)	0.9640(8)	0.045(2)
N3C	0.4213(3)	0.1290(3)	0.6253(8)	0.043(2)
N1	0.6382(3)	0.1533(4)	0.5079(7)	0.045(2)
C5	0.6182(3)	0.1406(3)	0.4117(9)	0.051(2)
C3	0.7081(3)	0.1431(4)	0.3910(7)	0.078(3)
C2	0.6951(3)	0.1558(4)	0.4967(7)	0.082(3)
H2A	0.7212(3)	0.1645(4)	0.5507(7)	0.099
N3	0.6360(4)	0.3410(4)	1.0876(7)	0.049(2)

TABLE 3.4.1(b) Bond Angles in $Zn(Im)_2$

Atoms	Angle (°)	Atoms	Angle (°)
N3B-Zn1-N3C	111.7(3)	C5B-N1B-Zn2	126.8(6)
N3B-Zn1-N3	105.8(4)	N3C-C2C-N1C	114.6(9)
N3C-Zn1-N3	109.7(4)	N1A-C2A-N3A	117(1)
N3B-Zn1-N1A	116.4(3)	C4C-C5C-N1C	112.2(9)
N3C-Zn1-N1A	108.7(4)	C4B-C5B-N1B	108.2(7)
N3-Zn1-N1A	104.1(4)	N3A-C4A-C5A	109(1)
N1C-Zn2-N1B	114.0(3)	C5C-C4C-N3C	108(1)
N1C-Zn2-N3A	110.3(3)	C5B-C4B-N3B	109.6(7)
N1B-Zn2-N3A	105.4(4)	N1A-C5A-C4A	108(1)
N1C-Zn2-N1	107.7(4)	C2A-N3A-C4A	103.3(9)
N1B-Zn2-N1	112.3(4)	C2A-N3A-Zn2	127.7(8)
N3A-Zn2-N1	107.0(3)	C4A-N3A-Zn2	128.2(8)
C2C-N1C-C5C	101.6(8)	C2C-N3C-C4C	103.0(9)
C2C-N1C-Zn2	126.5(7)	C2C-N3C-Zn1	124.7(8)
C5C-N1C-Zn2	131.7(7)	C4C-N3C-Zn1	131.9(8)
C2A-N1A-C5A	103.8(9)	C5-N1-C2	105.6(8)
C2A-N1A-Zn1	131.8(8)	C5-N1-Zn2	126.9(7)
C5A-N1A-Zn1	124.2(8)	C2-N1-Zn2	125.5(7)
C2B-N3B-C4B	104.2(7)	N1-C5-N3	113.0(6)
C2B-N3B-Zn1	129.8(7)	N3-C3-C2	108.0(8)
C4B-N3B-Zn1	126.0(6)	N1-C2-C3	107.9(8)
N3B-C2B-N1B	113.9(7)	C5-N3-C3	105.3(8)
C2B-N1B-C5B	103.9(7)	C5-N3-Zn1	125.6(7)
C2B-N1B-Zn2	129.2(7)	C3-N3-Zn1	126.3(7)

TABLE 3.4.1(c) Bond Lengths in $Zn(Im)_2$

Atoms	Bond Length (Å)
Zn1-N3B	1.976(7)
Zn1-N3C	1.978(8)
Zn1-N3	1.985(9)
Zn1-N1A	1.990(8)
Zn2-N1C	1.950(7)
Zn2-N1B	1.971(8)
Zn2-N3A	1.992(9)
Zn2-N1	2.001(9)
N1C-C2C	1.34(1)
N1C-C5C	1.34(1)
N1A-C2A	1.29(1)
N1A-C5A	1.35(1)
N3B-C2B	1.32(1)
N3B-C4B	1.344(9)
C2B-N1B	1.33(1)
N1B-C5B	1.364(9)
C2C-N3C	1.33(1)
C2A-N3A	1.32(1)
C5C-C4C	1.31(1)
C5B-C4B	1.340(8)
C4A-N3A	1.33(1)
C4A-C5A	1.38(1)
C4C-N3C	1.37(1)
N3A-Zn2	1.992(9)
N3C-Zn1	1.978(8)
N1-C5	1.32(1)
N1-C2	1.34(1)
C5-N3	1.33(1)
C3-N3	1.34(1)
C3-C2	1.380(9)
N3-C5	1.33(1)
N3-C3	1.34(1)

FIGURE 3.4.1(a) Ortep Diagram at 50% Probability of the Asymmetric Unit of $Zn(Im)_2$

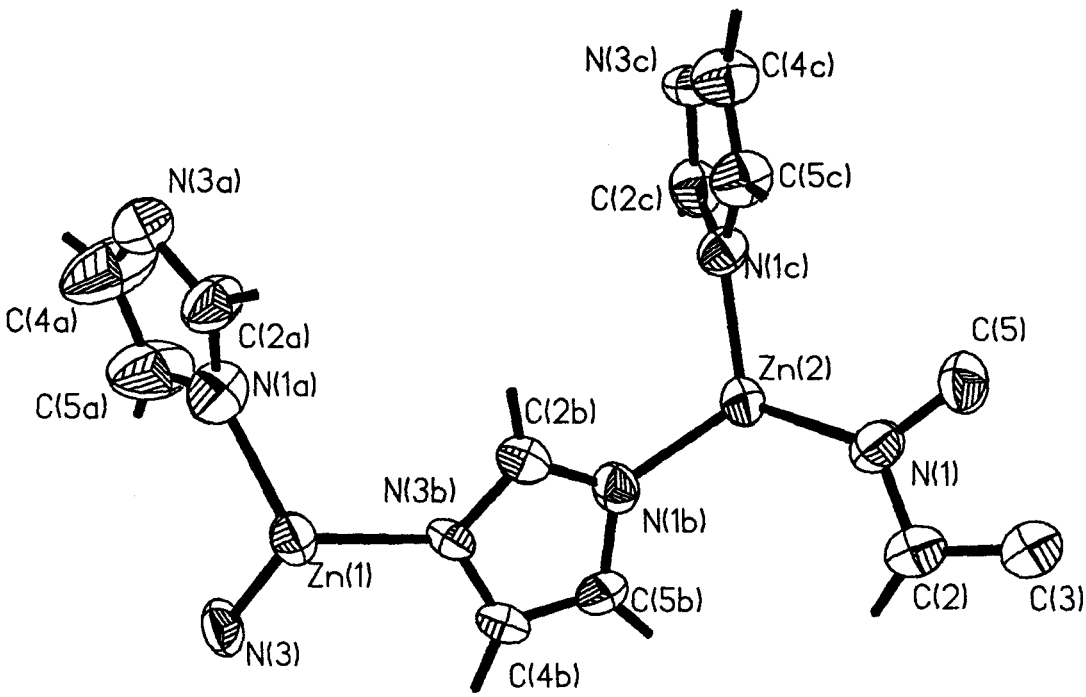

FIGURE 3.4.1(b) Stereoview of the Molecular Packing in $Zn(Im)_2$ as Viewed Down the [001] Axis

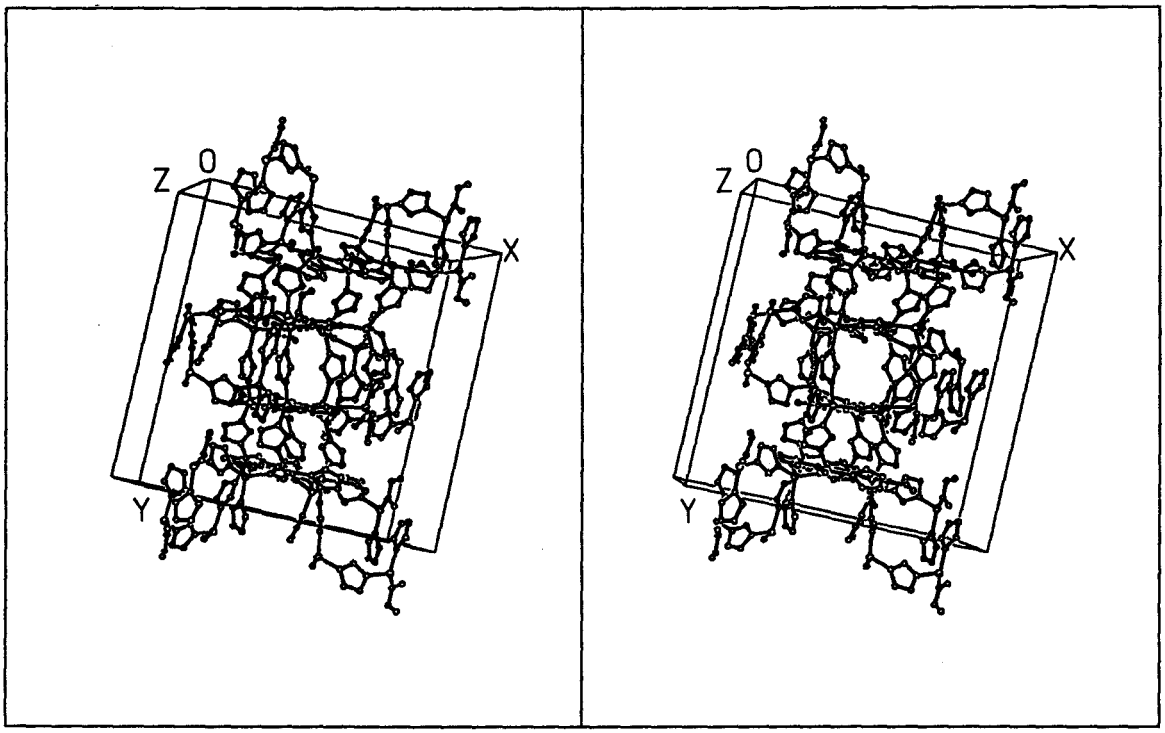

The hydrogen atoms have been omitted for clarity.

FIGURE 3.4.1(c) Molecular Packing Diagram of $Zn(Im)_2$ Illustrating Tetrahedral Coordination of Zn Atoms (as Viewed Down the [100] Axis)

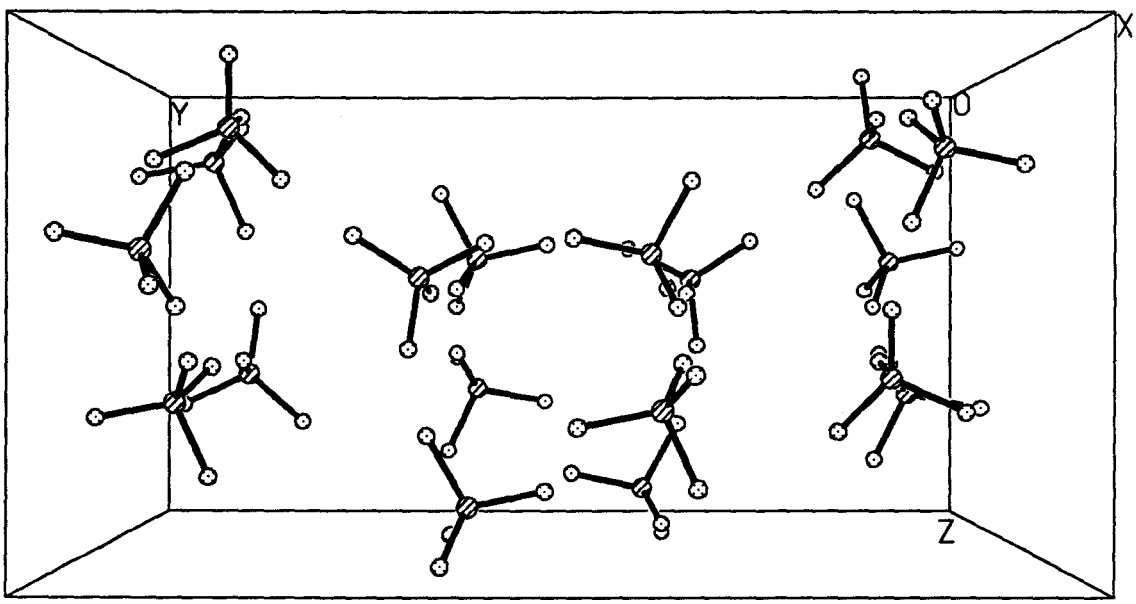

The carbon and hydrogen atoms have been omitted for clarity. The zinc atoms are located at the centre of the tetrahedra and are shown as circles with diagonal lines. The nitrogen atoms are located at the apices of the tetrahedra and are shown as circles with dots.

3.5 Vibrational Spectroscopy Of Zinc And Copper Compounds

Table 3.5 tabulates and compares the infrared frequencies for the compounds studied in this thesis. Figures 3.5 (a-d) show the infrared spectra collected for the compounds studied in this work.

Table 3.5 Infrared Frequencies[§§]

$ImBr_3H{\cdot}OAc$ (I)	$Zn(ImBr_3)_2(OH_2)_2$ (II)	$Zn(ImBr_3)_2(OD_2)_2$ (II-D)	$Zn(Im)_2$ (III)	$Cu(ImBr_3)_2(OH_2)_2$ (IV)
3440 w	3378 m	3423 br, w	3425 br, w	3424 br, w
3072 m	3334 m	3349 br, w		3339 m
3007 s	3240 w			3277 m
2921 s	3190 w			3201 m
2840 sh, m	3130 w			3123 m
2814 s				2926 sh, w
2733 m				2856 sh, w
2711 m		2517 m		
2618 m		2476 m		
2416 w		2364 w		
		2330 w		
		2301 w		
1651 w			1666 w	
	1615 sh, w		1612 w	1612 m
1533 s	1603 m			
			1497 s	
1443 m	1480 m	1480 m	1473 m	1479 m
1394 s	1384 s	1384 s	1321 m	1385 s
1298 m	1289 s	1288 s	1290 w	1299 m
	1245 sh. m	1260 sh, w		1265 s
	1228 s	1245 m	1240 m	1201 s
1185 m	1190 s	1201 s		1026 s
1004 m	1106 s	1170 sh, w	1171 m	985 s
980 s	979 s	1027 s	1038 s	755 br, w
838 m	694 s	979 s	953 s	575 m
667 w	669 sh, m	946 s	833 m	416 m
	630 w	680 w	775 sh, m	
	610 w	526 m	758 s	
			668 s	

[§§] Values are in cm^{-1}. Abbreviations are: s = strong; m = medium; w = weak; sh = shoulder. Intensity of band is relative to other bands in the same spectrum. All values are from baseline adjusted spectra.

FIGURE 3.5(a) Infrared Spectrum of $ImBr_3H{\cdot}OAc$

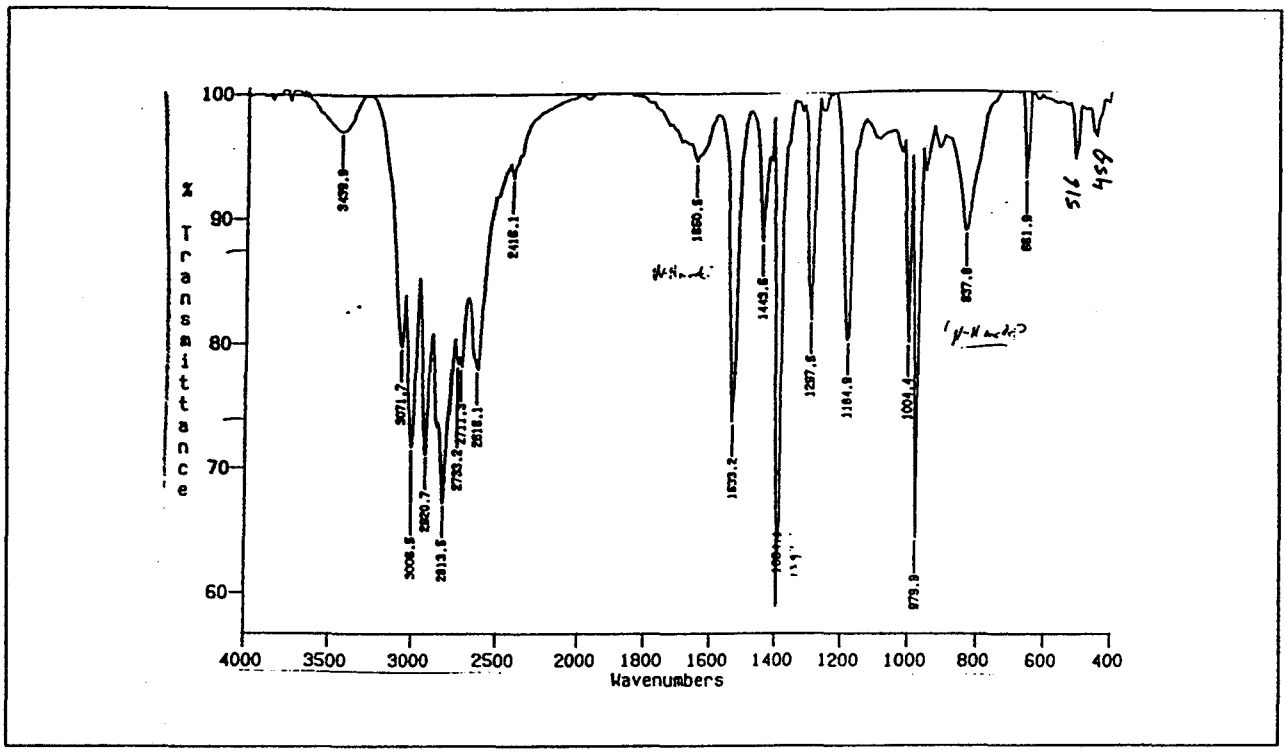

FIGURE 3.5(b) Infrared Spectrum of $Zn(ImBr_3)_2(OH_2)_2$

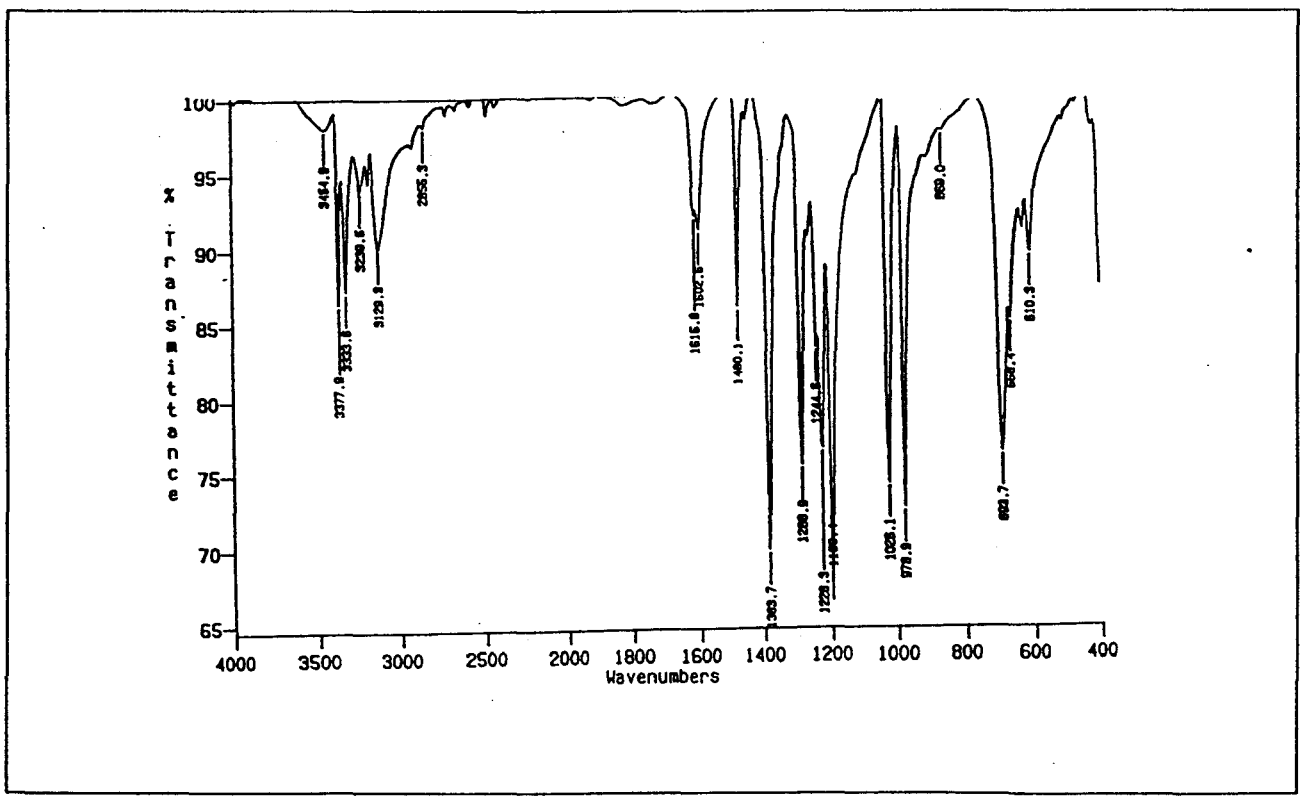

FIGURE 3.5(c) Infrared Spectrum of $Zn(ImBr_3)_2(OD_2)_2$

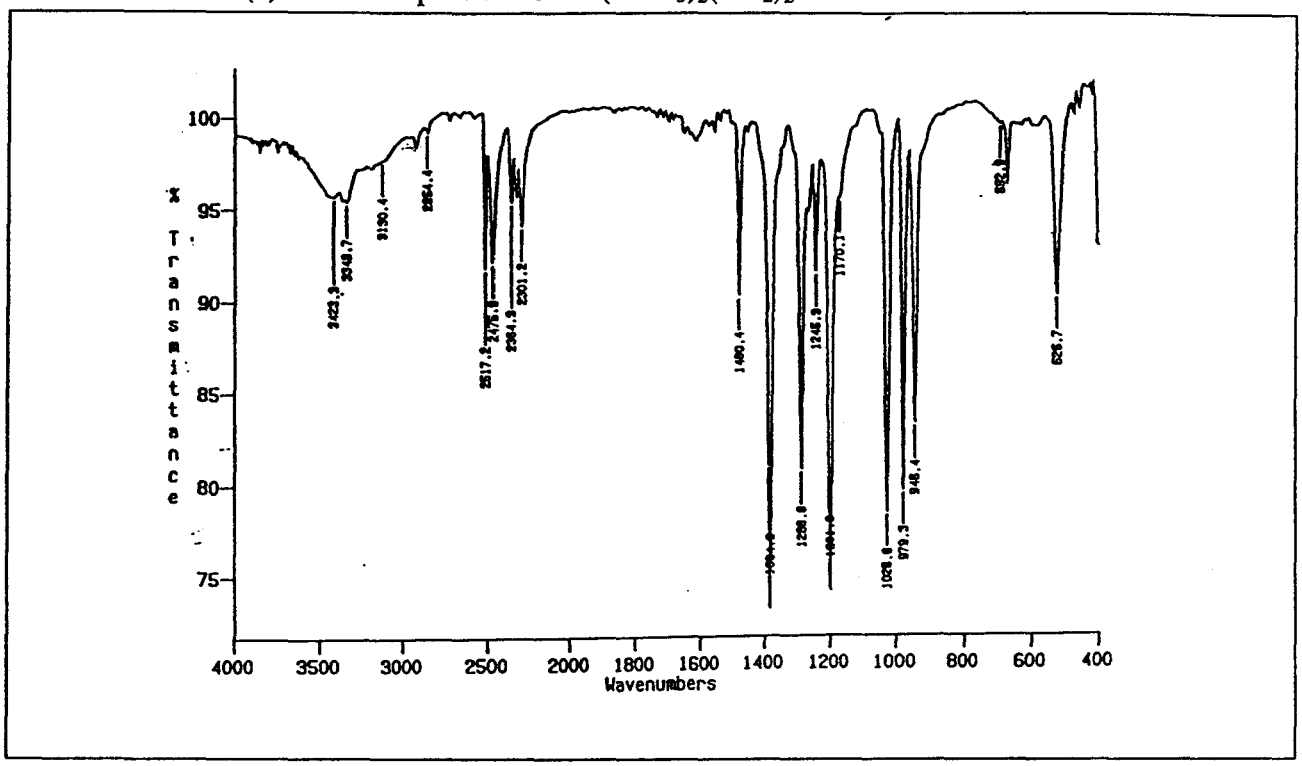

FIGURE 3.5(d) Infrared Spectrum of $Zn(Im)_2$

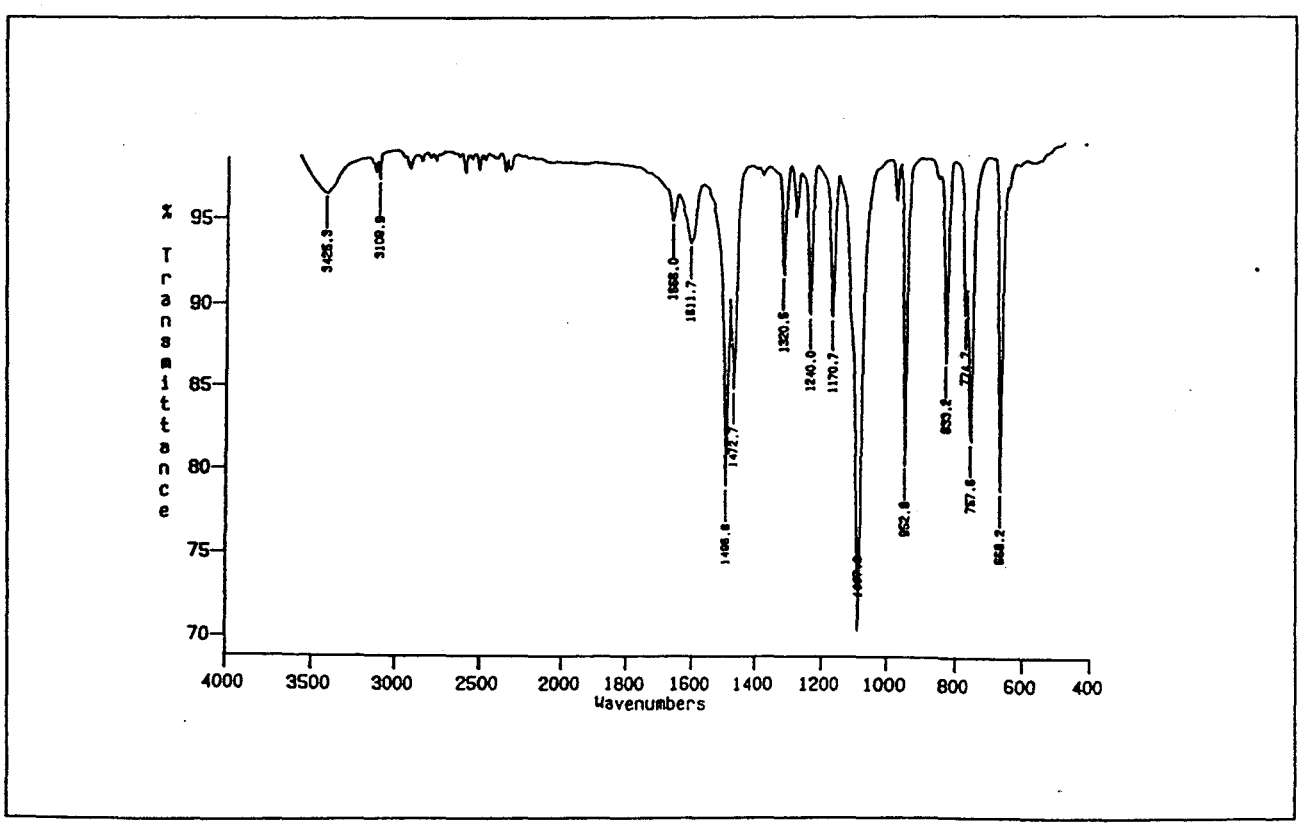

FIGURE 3.5(e) Infrared Spectrum of $Cu(ImBr_3)_2(OH_2)_2$

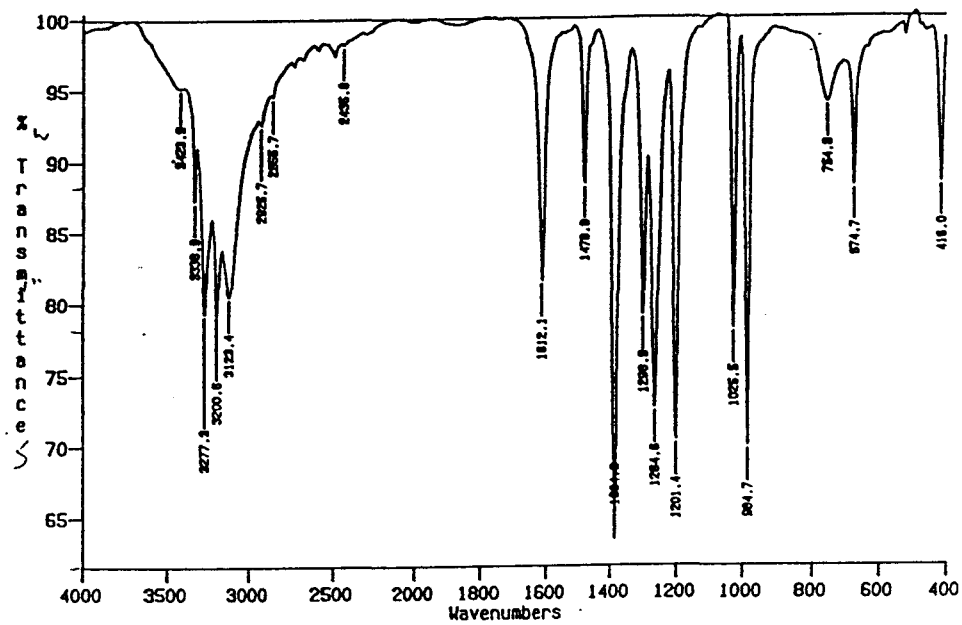

4. DISCUSSION

4.1 Triaquo(tris-2-pyridylphosphine)nickel(II) dinitrate

The structure of triaquo(tris-2-pyridylphosphine)nickel(II) dinitrate is very similar to that of its zinc analogue. Both the nickel and zinc compound are six coordinate with a regular octahedral geometry. Three of the coordination sites are occupied by the nitrogen atoms of the pyridyl rings and three of the coordination sites are occupied by the oxygen atoms of water molecules. The metal nitrogen bonds are shorter in the nickel compound (2.05(1) Å for the nickel compound versus 2.126(3) Å for the zinc compound). The metal oxygen bonds are comparable for the two compounds, with each compound showing a variety of bond lengths (compare the metal oxygen bond lengths in the nickel compound from Table 3.1(b) with the metal oxygen bond lengths for the zinc compound which are (in Å): 2.075(3), 2.152(3), 2.110(3)). The corresponding bond angles and lengths for the ligand are not significantly different between the two compounds.

4.2 Bis(2,4,5-tribromoimidazole)(diaquo)zinc(II)

4.2.1 Geometrical Features of $Zn(ImBr_3)_2(OH_2)_2$

One of the oxygen-hydrogen bonds of the zinc coordinated water molecule has a bond length of 1.18(5) Å which is slightly longer than the oxygen-hydrogen bond length of an uncoordinated water molecule [0.97(1)]. The presence of longer oxygen-hydrogen

bonds is no surprise since one of the biological roles of zinc has been assumed to be the lowering of the pKa of water. Weaker, and therefore longer, bonds would be associated with a lower pKa for water. In this respect, (**II**) is a successful model of zinc enzymes.

4.2.2 Comparison With Other Zinc Imidazole Compounds

One of the first difficulties in elucidating the structure of (**II**) was determining whether the compound was a perhydroxo compound, a peraquo compound, or a mixed aquo-hydroxo compound. X-ray crystallography is ill suited for locating hydrogen atoms because the scattering factor of an atom is proportional to its atomic number. Since our structure has bromine atoms, only the most ideal conditions would have allowed us to define the hydrogen atom positions from X-ray data alone.

A comparison of the zinc-nitrogen bond lengths and angles (Table 4.2.2) with a series of zinc imidazole compounds in which the imidazole groups are successively protonated (from $Zn(Im)_2$ in which the coordinated imidazole groups are both deprotonated to $Zn(Im)_2^{2+}$ in which coordinated imidazole groups are both protonated) allowed us no conclusions about the protonation of the imidazole group in (**II**).

A search of the Cambridge Crystallographic Database and the Inorganic Crystal Database produced 28 compounds similiar in structure to (**II**). The zinc-oxygen bond length ranged from 1.984(1) Å to 2.20(6) Å. The zinc-oxygen bond in (**II**) is slightly

longer than most compounds but not distinct enough to allow us to unambiguously choose which tautomeric form of (**II**) we had synthesized.

Table 4.2.2 A Comparison Of The Bond Lengths And Angles Involving Zinc And Nitrogen Atoms For A Series Of Zinc Imidazole Compounds

	$Zn(ImBr_3)_2(OH_2)_2$	$Zn(Im)_2$	$Zn(ImH)_2(Im)^+$	$Zn(Im)_2^{2+}$
N-Zn-N (°)	109.2(4)	104.1(4) to116.4(3)	105.9(1) to 111.5(1)	105.2(5)
Zn-N (Å)	2.008(6)	1.950(7) to 2.001(9)	1.986(3) to 2.000(3)	2.02(1)

4.2.3 Vibrational Spectroscopy

Vibrational spectroscopy was considered as a probe to determine whether (**II**) was a peraquo or a perhydroxo species. Towards this end, a deuterated analogue of (**II**), (**II-D**) was synthesized. (**II-D**) was prepared under the same conditions as (**II**), with the exception that deuterated starting materials were used; furthermore, the X-ray powder diffraction patterns of the two compounds were identical, allowing us the assumption that they were alike in all respects except for the substitution of deuterium for hydrogen.

The vibrational spectrum of (**II-D**) was recorded and is shown along with the vibrational spectrum of (**II**) in Figure 3.5(c). Several bands in (**II**) showed a very clear shift with a ratio $[(\mathbf{II})_\nu/(\mathbf{II\text{-}D})_\nu]$ of approximately 1.3. The relevant bands and the frequencies to which they shifted upon deuteration are shown below in Table 4.2.3.

The results shown below are suggestive of the aquo species, but still do not provide definite proof.

TABLE 4.2.3- Infrared Bands in $Zn(ImBr_3)_2(OH_2)_2$ and $Zn(ImBr_3)_2(OD_2)_2$

$Zn(ImBr_3)_2(OH_2)_2$ *(cm^{-1})*	$Zn(ImBr_3)_2(OD_2)_2$ *(cm^{-1})*	*Assignment*
3378 m	2517 m	O-H stretch*
3334 m	2476 m	O-H stretch*
3240 w	2365 m	O-H stretch*
3175, w	2330, w	O -H stretch*
3130 w	2301 m	O-H stretch*
1616 sh,w and 1602 w	buried under other peaks	H-OH bend
1228 s	946 s	O-H libration
693 s	527 m	O-H libration

4.2.4 Application Of Bond Valence Theory

Our next recourse for trying to determine whether **(II)** was a peraquo or a perhydroxo species was bond valence theory. Bond valence theory was developed at McMaster University by I. D. Brown[47]; it is an empirical application of graph theory to bonding interactions in solid state materials. Essentially, Brown has set up an accounting system which allows one to determine how many bonding interactions to expect for an individual atom. Equation 4.2.4(a) is used to determine bond valence

$$s = \exp [(R_o-R)/B] \qquad \text{Equation 4.2.4(a)}$$

*One of these bands is probably an overtone of the HOH bend, possibly Fermi coupled to one of the O-H stretches

where s is the bond valence, R is the bond length, and R_o and B are empirically determined constants. The sum of bond valence values for an individual atom will be equal to that atom's valence. The empirical constants have been determined by applying the model to compounds in the inorganic crystal database.

Brown has compiled a large number of constants for metal-oxygen and metal-nitrogen bonds, which is ideal for the problem at hand. Table 4.2.4 below shows the empirical constants, bond lengths, and resulting bond valence values from Equation 4.2.4(a) when bond valence theory was applied to **(II)**.

Table 4.2.4 Bond Valence Calculations

Bond	*Length (Å)*	R_o	*B*	*s*
Zn-N	2.008	1.767	0.37	0.52
Zn-O	2.022	1.704	0.37	0.42

The sum of the above s values for each bond is shown below:

$$2(\text{Zn-N}) + 2(\text{Zn-O}) = \text{valence of zinc}$$

$$2(0.52) + 2(.42) \approx 1.9$$

It is now possible to determine what the oxygen-hydrogen bond length will be for both the hydroxo and aquo species. If we take the valence of oxygen as 2, then the balance of the valence for the zinc bound oxygen, 1.6. This value implies that the

compound exists as a peraquo species, since hydrogen can not have a valence higher than unity. This calculation was confirmed by the single crystal neutron diffraction study.

4.2.5 Neutron Diffraction Study

The single crystal neutron data gave a result for the hydrogen atoms which was, at first, somewhat puzzling. We had expected to find either one or two protons bonded to the oxygen atom (representing the hydroxo and aquo species, respectively); we were surprised when a result of three disordered protons, each with an occupancy of 0.67, was the answer which agreed best with diffraction data. Our interpretation of this result is that the aquo species was present, since 3 x 0.67 is approximately 2, the number of protons expected for an aquo species.

Another interesting feature of the disordered protons is their geometry. They are located at the vertices of a regular tetrahedron (with oxygen in the middle and zinc at one of the vertices). A similar tetrahedral geometry has been observed often for oxygen atoms: the ice structure, with its extensive hydrogen bonding network, consists of oxygen atoms surrounded in a tetrahedral fashion by protons[48].

The presence of the water molecules may be explained by the requirement that zinc complete its coordination sphere. Since water would be the species of highest

concentration in an aqueous solution, one would expect it to be the most likely candidate for the completion of the zinc coordination sphere. It is also worth considering that three of the weak bonding interactions are between the protons of the water molecule and the bromine atoms. The disorder of the water molecules is evidence of their role in intermolecular bonding. The zinc coordinated water molecule is quite flexible, allowing it to fulfill a wide variety of bonding geometries. If several of these geometries were isoenergetic, one would then expect a large amount of disorder for the water molecules.

4.2.6 An Examination Of The Imidazole Rings

Craven *et al.* (ref.57) had previously noted that no major changes occur within the imidazole ring upon protonation of the N3 nitrogen atom (see Figure 4.2.6 for standard notation on the imidazole ring). However, there are some changes which occur upon coordination to the zinc atom. In Tables 4.2.6(a-b), the structures of (**II**) and (**III**) have been compared with two other zinc-imidazole species: a catenated zinc species which consists of long chains of bisimidazole coordinated zinc atoms bridged by imidazolate atoms (with a nitrate counterion present), and dichloro(diimidazole)zinc(II). Crystallographic parameters for the imidazole and the imidazolium molecules are also presented.

Figure 4.2.6 Standard Notation for Imidazole Rings

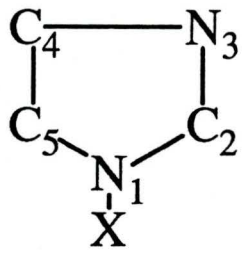

Numbering starts at the nitrogen atom which is bound to X (in the case of imidazole, X = H, and in the case of (**II**), X = Zn) and continues sequentially around the ring. For imidazolate in which the nitrogen is deprotonated, there is no differentiation between N1 and N2 or C4 and C5.

Table 4.2.6(a) Imidazole Ring Bond Lengths (Å)

Compound	N1-C2	C2-N3	N3-C4	C4-C5	C5-N1
$Zn(ImBr_3)_2(OH_2)_2$ (**II**)	1.341(9)	1.32(1)	1.36(1)	1.32(1)	1.356(9)
$Zn(Im)_2$ (**III**)- Ring 1***	1.32(1)	1.33(1)	1.34(1)	1.380(9)	1.34(1)
$Zn(Im)_2$ (**III**) - Ring A	1.39(1)	1.32(1)	1.33(1)	1.38(1)	1.35(1)
$Zn(Im)_2$ (**III**) - Ring B	1.33(1)	1.32(1)	1.344(9)	1.370(8)	1.364(9)
$Zn(Im)_2$ (**III**) - Ring C	1.34(1)	1.33(1)	1.37(1)	1.31(1)	1.34(1)
$Zn(ImH)_2^{2+}$	1.32(2)	1.35(2)	1.37(2)	1.37(2)	1.37(2)
$Zn(ImH)_2(Im)^+$ Ring A†††	1.316(6)	1.333(7)	1.347(8)	1.349(8)	1.381(6)
$Zn(ImH)_2(Im)^+$ Ring B	1.313(5)	1.320(6)	1.351(9)	1.370(7)	1.373(6)
$Zn(ImH)_2(Im)^+$ Ring C	1.318(5)	1.328(5)	1.352(6)	1.354(8)	1.342(7)
Imidazolium $(ImH)^{49}$	1.323(4)	1.333(4)	1.377(4)	1.335(4)	1.373(4)
Imidazole $(Im)^{50}$ ‡‡‡	1.337(3)	1.316(2)	1.367(2)	1.357(2)	1.362(2)

*** There are four different imidazole rings in the $Zn(Im)_2$ structure. The atoms of one of the rings have only a numerical labelling, while the other three are labelled A, B, C.

††† There are three crystallographically different imidazole groups in this structure. Ring A is protonated, rings B and C are deprotonated but coordinated to other zinc atoms, forming a catenated structure similar to $Zn(Im)_2$.

‡‡‡ This structure was determined from neutron diffraction data.

Table 4.2.6(b) Imidazole Ring Bond Angles (°)

Compound / Atoms	C5-N1-C2	N1-C2-N3	C2-N3-C4	N3-C4-C5	C4-C5-N1
$Zn(ImBr_3)_2(OH_2)_2$ (**II**)	101.6(6)	116.3(7)	101.9(6)	110.8(7)	109.4(6)
$Zn(Im)_2$ (**III**) - Ring 1	105.6(8)	113.0(6)	105.7(8)	108.0(8)	107.9(8)
$Zn(Im)_2$ (**III**) - Ring A	103.8(9)	116.4(1)	103.3(9)	109(1)	107.5(1)
$Zn(Im)_2$ (**III**) - Ring B	103.9(7)	113.9(7)	104.2(7)	109.6(7)	108.2(7)
$Zn(Im)_2$ (**III**) - Ring C	101.6(8)	114.6(9)	103.0(9)	108.3(1)	112.2(9)
$Zn(Im)_2^{2+}$	105.6(3)	110.5(3)	108.8(3)	103.7(3)	111.5(3)
$Zn(ImH)_2(Im)^+$ Ring A	105.4(4)	110.9(4)	108.1(4)	106.7(5)	108.8(5)
$Zn(ImH)_2(Im)^+$ Ring B	106.7(4)	111.1(4)	108.0(5)	106.8(5)	107.4(4)
$Zn(ImH)_2(Im)^+$ Ring C	104.7(4)	114.0(3)	103.8(4)	108.8(5)	108.6(5)
Imidazolium	108.7(2)	108.4(2)	108.2(2)	107.3(2)	107.4(2)
Imidazole	107.0(1)	112.0(1)	105.1(1)	109.8(1)	106.7(1)

In the structure of (**II**), the most pronounced changes are the C4-C5 bond shortening and the collapse of the angles around the nitrogen bonds. The C4-C5 bond length decrease is also reflected in the molecular orbital calculations (see Section 4.2.12), which indicated a relatively strong pi bond between the two carbon atoms. In the absence of crystallographic data for the tribromoimidazole molecule, it is difficult to tell whether this bond shortening is caused by the zinc atom or the bromine atoms. It is, however, worth noting that the orbitals responsible for this double bond (the carbon p_y orbitals) play a major role in the HOMO of (**II**). The HOMO plays a large role in determining the stability of a molecule.

The shortening of the carbon-carbon bond may be responsible for the decrease in the carbon-nitrogen-carbon bond angles, which in turn may change the hybridization of the nitrogen atoms. This would result in an alteration of the electron density on the nitrogen

atoms which would alter the pKa of the imidazole nitrogen atoms. This is illustrated below in Table 4.2.6(c) which shows the change in nitrogen pKa for a series of unsaturated amine bases in which the carbon-nitrogen-carbon angle gradually decreases.

Table 4.2.6(c) - pKa of Nitrogen Compounds

Compound	*pKa*	*C-N-C Bond Angle (°)*[§§§]
diethylamine	10.49	110.5(5)[51]
piperidine	11.12	111.2(8)[52]
pyrrolidine	11.27	104.1(5)[53]
azetidine	11.29	88.6(4)[54]

The imidazole group has been suggested as part of a catalytic triad consisting of a carboxylic acid group (a side chain for amino acids like glutamic acid) and the zinc atom. A subtle change in the imidazole nitrogen pKa values may result in a fine tuning of the triad's catalytic ability which may explain the prevalence of zinc-imidazole based enzymes in biological systems. As discussed in Section 4.2.9, the pKa of the imidazole group is important in catalytic biological systems.

4.2.7 The Stability Of $Zn(ImBr_3)_2(OH_2)_2$

Since compound (**II**) is a good starting point for the design and synthesis of further metalloenzyme models; it would be worthwhile to consider what enabled us to synthesize and crystallize it. The molecule is unique because it is the only bisimidazolate zinc species which does not form a polymer as observed in the $Zn(Im)_2$ compound. There are two

[§§§] The bond angles for diethylamine were determined from a clathrate compound. All other bond angles are from alkyl derivatives.

unique feature about **(II)**: the replacement of the imidazole hydrogen atoms with bromine atoms and the coordination of the water molecules to **(II)**. Water is present in the synthesis of any zinc imidazolate species from aqueous solution, so we must concentrate on the role of the bromine atoms in the stabilization of the structure.

There are two conceivable ways in which the bromine atoms could be influencing the stability of **(II)**. The first is their role in forming hydrogen bonding interactions throughout the crystal lattice. The second is their role in reducing the pKa of the nitrogen atoms in the imidazole ring.

4.2.8 Intermolecular Bonds

The intermolecular bromine bonds may help to stabilize the solid state structure, which for reasons of packing may favour the bisimidazole over any other coordination number. It may be that a zinc atom coordinated by three, four, or a higher number of tribromoimidazole molecules may also be stable. However, because of the insolubility of the species with two tribromoimidazole molecules, which would most likely form before the three or higher coordinated species, we obtain the **(II)** molecule as the principle product of the reaction.

There are three different intermolecular hydrogen bonds involving bromine atoms in the solid state structure of **(II)**. They are listed in Table 4.2.8 below:

Table 4.2.8 Hydrogen Bonding Interactions in $Zn(ImBr_3)_2(OH_2)_2$

Atoms	***Bond length (Å)***
Br_4 and H_{1BA}	2.69(5)
Br_2 and H_{1A}	2.55(5)
Br_4 and H_{1CA}	2.96(5)

Although these are weak bonding interactions in comparison with ionic or covalent bonds, one must remember that they extend throughout the crystal lattice. This effect would serve to enhance the ability of the weak bonds to stabilize the structure.

The insoluble nature of **(II)** in all but acidic solvents may also be evidence of the role that intermolecular bonds may be playing in the stability of the species. In order to dissolve a compound in a solvent, the solvent molecules must be able to interact strongly enough with the solute molecules to overcome the lattice energy. If the electron density of a molecule in the solid state was delocalized through a network of intermolecular bonds there would be fewer areas to which the solvent molecule would be able to coordinate. In short, the coordination energy of the solvent molecules with **(II)** would not be stronger than that of the energy gained by the intermolecular bonding. The net result would be insolubility, which was observed for **(II)**.

The solubility of (**II**) in acidic medium is most probably caused by protonation of the N3 nitrogen atom or perhaps the zinc bound oxygen atom. This would result in the formation of an ion, which could interact more favourably with solvating molecules.

Another piece of experimental evidence suggesting the presence of intermolecular bonding is the high melting point of **(II)** (>360°C). The high melting point is certainly caused, in part, by the ionic nature of the compound, but when compared to other ionic compounds with zinc-nitrogen bonds ($Zn(NO_3)_2 \cdot 6H_2O$ with a melting point of 297°C, the corresponding trihydrate with a melting point of 243°C, and Zn_3N_2 with a melting point of 224°C) it is still considerably high. The presence of intermolecular bonding is a plausible explanation for this elevated melting point.

4.2.9 The pKa of $ImBr_3$

The second pKa of imidazole is 14.5. This corresponds to the dissociation of the neutral species into a proton and an imidazolate ion. It is a measure of the capability of ring nitrogen atoms to bear a negative charge. In comparison to this is the tribromoimidazole molecule which has a second pKa of 10.7(2). This is lower than that of imidazole which means that the neutral species will dissociate more readily, which implies that the nitrogen atoms can more easily take on a formal negative charge. The word formal is used here because this negative charge is distributed over the bromine atoms of the tribromoimidazole molecule. The delocalization of the electron density reduces the negative charge on the nitrogen atoms, making it less favourable for them to bind to a second zinc atom in solution, thereby preventing the formation of polymeric chains of zinc-imidazolate species as observed for the $Zn(Im)_2$ species. This is a very subtle but also a very intriguing effect, one which has not been previously exploited in the synthesis of zinc enzyme models.

Christianson and Alexander[55] have examined the effect of lowering the electron density on the nitrogen atoms of imidazole rings (as part of histidine residues) bound to zinc in metalloenzymes. On the basis of known protein structures and homologues thereof, they found thirty examples of what they dubbed indirect carboxylate zinc coordination (the term indirect is used because the coordination was through a bridging

imidazole group), which they identified as a carboxylate-histidine-zinc catalytic triad. The carboxylate modifies the pKa of the system by withdrawing electron density from the zinc atom through the N3 atom of the imidazole group, thereby tuning the zinc atom for its biological role. It is significant that all of the examples they found were catalytic zinc sites (see section 1.9.1).

Recall that all catalytic zinc sites involve the coordination of a water molecule to the zinc atom, similar to the coordination of water to zinc in **(II)**. The bromine atoms of the tribromoimidazole rings in **(II)** could be acting in a manner analogous to the carboxylate groups in the carboxylate-histidine-zinc triad. By withdrawing electron density from the imidazole ring, the bromine atoms are lowering the electron density on the nitrogen atoms and thereby lowering the electron density available to the zinc atom.

The correspondence between the pKa effect of the bromine atoms and the indirect carboxylate interaction is further evidence that the pKa effect of the bromine atoms is a factor in the stability of **(II)**; especially so when one considers that **(II)** is structurally similar to the biological zinc species even though no steric restraints were used to obtain this similarity. The brominated imidazole group is therefore a good ligand for making models of the metal-imidazole interaction which is found in biological systems. Imidazole species with varying number and types of halogen atoms, or perhaps even other electron

withdrawing groups such as the nitro or alkoxy groups are synthetically accessible. This opens up possibilities towards further chemical modeling of biological zinc species.

4.2.10 Molecular Orbital Calculations For $Zn(ImBr_3)_2(OH_2)_2$

Extended Huckel Molecular Orbital (EHMO) calculations were carried out with the CACAO software package to illuminate the stability and bonding within **(II)**. The energy difference between the highest occupied molecular orbital (HOMO) and the lowest unoccupied molecular orbital (LUMO) is a good measure of the stability of a compound[56]. Stable compounds generally have a large HOMO-LUMO gaps, and the stability of any two similar compounds can be evaluated by comparing their HOMO-LUMO gap. Since the calculations here were carried out on **(II)** as a molecule rather than **(II)** as a solid state compound, no intermolecular interactions were considered.

Figure 4.2.10(a) shows a Walsh diagram from a series of calculations in which the tribromoimidazole **(I)** ligands were moved outwards from the central zinc atom. **(I)** was treated as having a single negative charge while the zinc atom was treated as having a double positive charge. The zinc-nitrogen bond length was varied from 1.5 Å to 2.5 Å over five steps (1.50 Å, 1.75 Å, 2.008 Å, 2.25 Å, and 2.50 Å). Figures 4.2.10(c-d) illustrate the change in geometry as well as the change in the HOMO.

FIGURE 4.2.10(a) - Energy Level Diagram For The Molecular Orbitals Of $Zn(ImBr_3)_2(OH_2)_2$

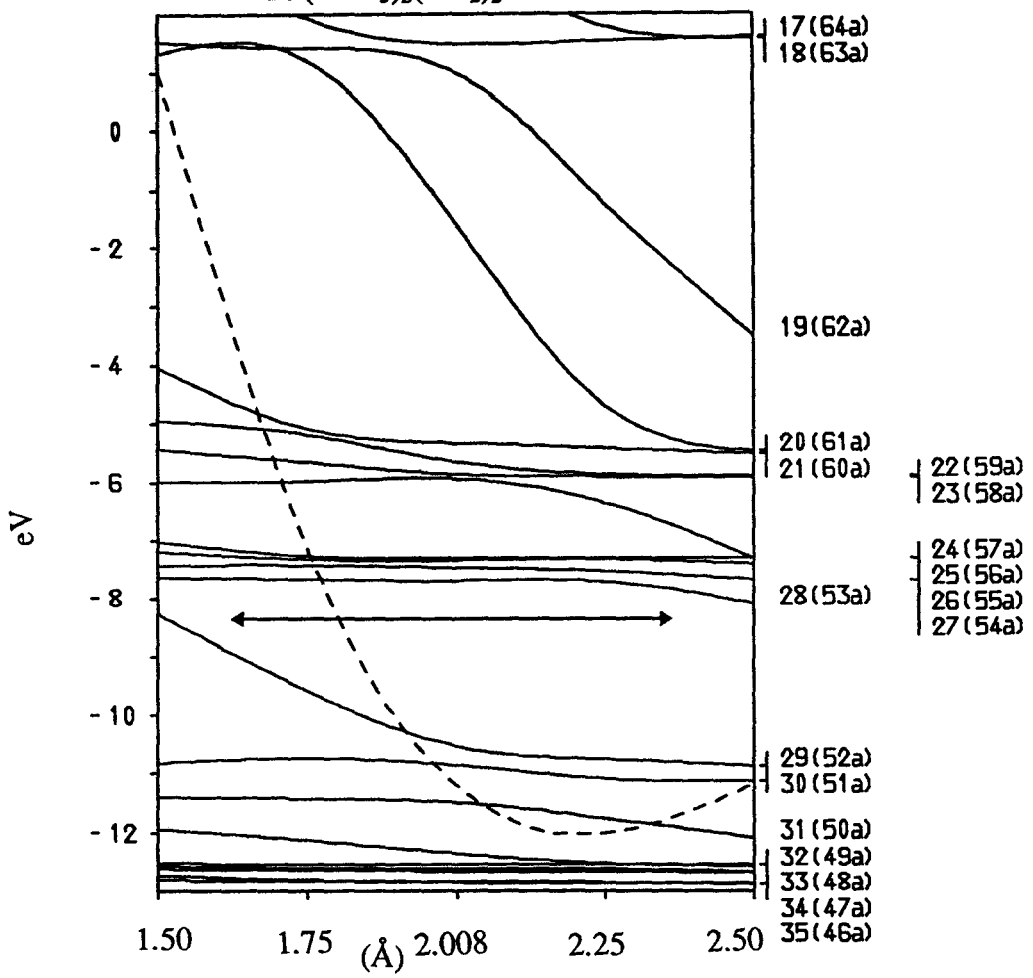

The y-axis indicates the energy of the molecular orbitals in eV while the x-axis indicates the lengths of the zinc-nitrogen bond. The solid lines indicate the energy of individual molecular orbitals. The dotted line indicates the overall energy of the complex. The scale for the overall energy is not shown. The double-headed arrow indicates the boundary between the filled and unfilled orbitals. The HOMO is directly below the double headed arrow while the LUMO is directly above.

The geometry of **(II)** as determined from the crystal structure can be found on the curve exactly where the HOMO reaches a lower limit plateau of approximately -11 eV. The HOMO, depicted in Figure 4.2.10(c), consists largely of the p_y orbital from the

bromine atom closest to the other imidazole ring. As is shown in Figure 4.2.10(b), a significant interaction between the orbitals of this bromine and the other ring occur when the zinc nitrogen bond is shortened. This suggests that the relatively large bromine atoms are responsible for the torsion angle observed between the two imidazole rings.

Another interesting result from the EHMO analysis is the shortening of the C4-C5 bond. Figure 4.2.10(d) shows that the p_y orbitals for these atoms are in phase for the shortened bonds and out of phase for the lengthened bonds (N3-C4 and C5-N1). This feature of the bonding within the imidazole ring is maintained as the ring approaches the zinc atom, with the exception of the N1 p_y orbital. Presumably, the electron density is flowing from this orbital to the sp^3 hybridized orbitals of the zinc atom.

In order to study the effect of the substitution of bromine for hydrogen in (**II**) further, calculations were performed on an analogue of (**II**) in which the bromine atoms were replaced with hydrogen atoms. The carbon-hydrogen bond lengths (1.1 Å) were taken from a neutron determination of the crystal structure of imidazole[57]. The results are tabulated in Table 4.2.10.

Table 4.2.10 A Comparison of the HOMO-LUMO Gap for $Zn(ImBr_3)_2(OH_2)_2$ and its Hydrogen Analogue

	$Zn(ImBr_3)_2(OH_2)_2$	$Zn(Im)_2(OH_2)_2$
HOMO ENERGY (eV)	-10.52	-12.16
LUMO ENERGY (eV)	-7.68	-7.88
DIFFERENCE (eV)	2.84	4.28

The difference of approximately 1.4 eV, corresponding to approximately 150 kcal/mol is a considerable value. The difference in the band gap energies is largely caused by the difference in the HOMO energies of the two molecules. This can be rationalized by examining the HOMO diagrams, shown in Figures 4.2.10(a-c). The large p_y orbitals on the bromine atoms are out of phase with the p_y orbitals of the carbon atoms to which they are joined. A phase difference between two adjacent orbitals will lead to a destabilization and therefore higher energy for an individual MO. The hydrogen atoms do not possess p orbitals, and therefore could not be out of phase with the carbon p_y orbitals.

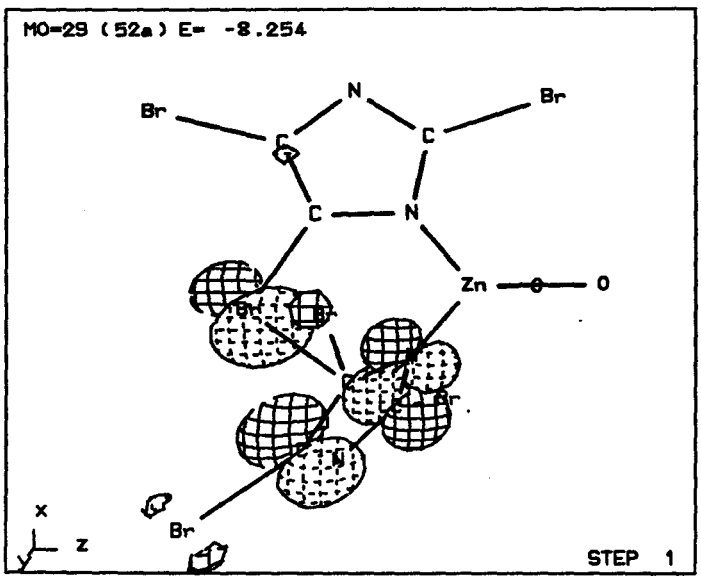

Fig 4.2.10(b) HOMO of $Zn(ImBr_3)_2(OH_2)_2$ with zinc nitrogen distance of 1.5 Å. Hydrogen atoms have been omitted for clarity. The phase of the orbitals is indicated by the two different types of cross-hatching. The top imidazole ring is contained within the X-Y plane.

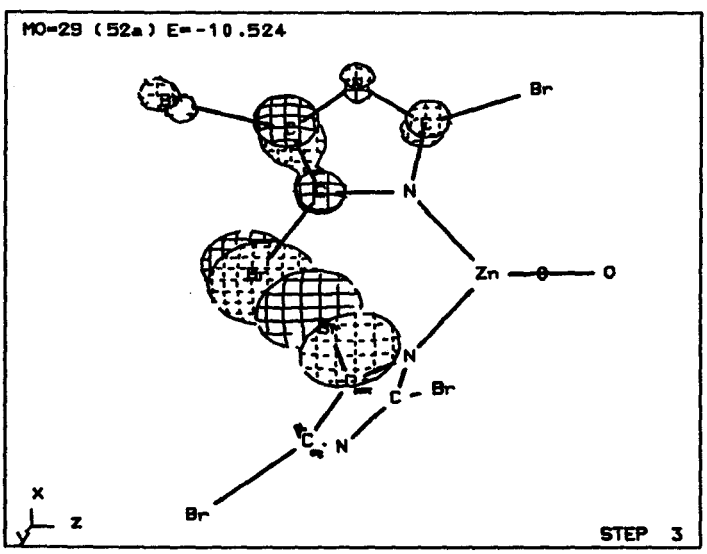

Fig 4.2.10(c) As in Fig. 4.2.10(b)except the zinc nitrogen distance is 2.008, the distance found from the X-ray crystal structure.

Fig 4.2.10(d) As in Fig. 4.2.10(b) except the zinc-nitrogen distance is 2.50 Å.

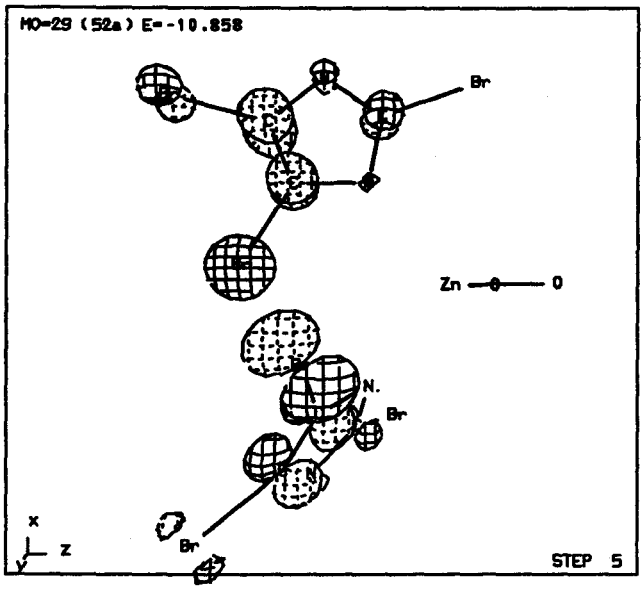

4.3 Bis(2,4,5-tribromoimidazole)(diaquo)copper(II)

A copper analogue of (**II**) has been synthesized. Copper is also an important metal for bioinorganic chemistry, and, like zinc, can be found ligated to histidine residues. Like (**II**), the copper species is insoluble. The copper species precipitates from the reaction mixture as birefringent red/green crystals. Thus far, we have been unsuccessful in obtaining crystals suitable for X-ray diffraction studies.

Elemental analysis (see Section 2.6.5) showed that a formulation similar to (**II**), namely $Cu(ImBr_3)_2(OH_2)_2$ was feasible. The only value which did not agree is the nitrogen percentage; however, this value was in error for the elemental analysis of (**II**) and may not be reliable. The metal percentage was also somewhat different from expected values but this value was also in error for (**II**) and also may not be reliable.

The vibrational spectrum of the copper analogue shows many features which are similar to **(II)**. These are presented in Table 3.5 and Figure 3.5(e). A square planar geometry is to be expected for this compound by analogy to other nitrogen ligated copper (II) compounds.

5. Appendix A - Partial Crystallographic Analysis of Tris(2-ethyl-1-methylimidazol-2-yl)phosphinenickel(II) dichloride

The compound was synthesized and crystallized by Z. Wang (see Reference 1).

The model structure could not be refined satisfactorily from the X-ray data. It is assumed that the crystal decomposed either before or during the data collection process. The crystals were observed to undergo a colour change from green to orange when exposed to low heat (the fiber optic light on the microscope stage was enough to cause the decomposition). Careful handling of the crystals before data collection followed by a low temperature data collection should provide adequate data for a satisfactory refinement of the structure.

Initial results indicate that the nickel atom is ligated by the N3 nitrogen atoms of the imidazole rings and either two or three water molecules. A summary of the crystallographic parameters is given in Table A5.

Table A5

Crystallographic Parameters for Tris(2-ethyl-1-methylimidazol-2-yl)phosphinenickel(II) dichloride

Formula / Formula weight	$C_{18}Cl_2H_{27}N_6NiP$ / 488.02
Crystal colour / Shape	green / irregular
Space Group / Cell Setting	Pnnm / Orthorhombic
Incident Radiation (Å)	Mo K_α (0.71073)
Unit cell parameters (Å and degrees)	a = 17.630(4) b = 18.670(4) c = 27.930(6)
	$\alpha = \beta = \gamma = 90.00$
Volume ($Å^3$) / Z	9192(3) / 17
ρ_{calc} (Mg m^{-3})	1.508
2θ Range (degrees)	$3 \leq 2\theta \leq 50$
Indices Range	$-1 \leq h \leq 20, -1 \leq k \leq 22, -1 \leq l \leq 33$
Temperature (°C)	22(1)
Standards / Decay	3 standards checked every 97 measurements
	showed a decay of 8%
# of Reflns Measured	8922/ 7417
R_{int}	0.16
F(000)	4369.0
R / R_w	0.30 / 0.45

6. Appendix B - Cacao Input Files

There were three different input files used to run the calculations for the Cacao suite of programs. File (1) is an input file which uses the crystallographic coordinates directly. File (2) uses the Z-matrix reference system to define the atomic positions; File (2) was used to generate the Walsh diagram in Section 4.2.10 as well as Figures 4.2.10.(b-d). File (3) was used to generate the HOMO-LUMO gap for the non-brominated analogue of (II).

FILE 1

```
# ZIMBR FROM XTAL COORDINATES
 23  0DIST  0  0  0
 EL CM RO NC WF HM OP OV
CELL 11.440,15.348,9.547,90.0,90.0,90.0
 0.00000,0.00000,0.70995,  *
 0.04120,0.09707,0.84436,  O
-0.12803,0.04763,0.58808,  N
-0.24166,0.02872,0.57153,  C
-0.29824,0.07449,0.47686,  N
-0.21373,0.12908,0.43000,  C
-0.11301,0.11271,0.49246,  C
-0.31635,-0.05650,0.67958, BR
-0.24367,0.21351,0.29177, BR
 0.03131,0.17002,0.47183, BR
 0.08400,0.15890,0.82230,  H
 0.05380,0.05800,0.96200,  H
-0.04120,-0.09707,0.84436,  O
 0.12803,-0.04763,0.58808,  N
-0.08400,-0.15890,0.82229,  H
-0.05380,-0.05800,0.96199,  H
 0.24166,-0.02872,0.57153,  C
 0.11301,-0.11271,0.49246,  C
 0.29824,-0.07449,0.47686,  N
 0.31635,0.05650,0.67958, BR
 0.21373,-0.12908,0.43000,  C
-0.03131,-0.17002,0.47183, BR
 0.24367,-0.21351,0.29177, BR
ZN  2  4 2.010-12.41  4 1.700 -6.53
```

FILE 2

```
# ZIMBR FROM Internal ref COORDINATES
 23  0DIST  0  1  5
1.5,1.75,2.008,2.25,2.5
 EL CM RO NC WF HM OP OV
0.0,0.0,0.0, *
1,2, N 1000,54.6,0
2,3, C 1.34,-134.1,0
3,4, N 1.31,116.3,0.0
4,5, C 1.35,101.9,0.0
5,6, C 1.32,110.8,0.0
3,7,BR 1.872,-121.9,0.0
5,8,BR 1.88,-121.8,0.0
6,9,BR 1.88,-129.0,0.0
1,10, N 1000,-54.6,0
10,11, C 1.34,-134.1,119.2
11,12, N 1.31,116.3
12,13, C 1.35,101.9
13,14, C 1.32,110.8
11,15,BR 1.872,-121.9
13,16,BR 1.88,-121.8
14,17,BR 1.88,-129.0
1,18, O -2.022,-50.2,90
1,19, O -2.022,50.2,90
18,20, H -1.21,-128.6
18,21, H -1.28,103.7
19,22, H -1.21,-128.6
19,23, H -1.28,103.7
ZN  2  4 2.010-12.41  4 1.700 -6.53
FMO  0
 DI WF CM RC
2,1,8,2,-1
```

FILE 3

```
# ZIMBR FROM Internal ref COORDINATES; HYDROGEN REPLACED WITH BROMINE
 23  0DIST  0  0  0
 EL CM RO NC WF HM OP OV
0.0,0.0,0.0, *
1,2, N 2.0220,54.6,0
2,3, C 1.34,-134.1,0
3,4, N 1.31,116.3,0.0
4,5, C 1.35,101.9,0.0
5,6, C 1.32,110.8,0.0
3,7, H 1.090,-121.9,0.0
5,8, H 1.09,-121.8,0.0
6,9, H 1.09,-129.0,0.0
1,10, N 2.022,-54.6,0
10,11, C 1.34,-134.1,119.2
11,12, N 1.31,116.3
12,13, C 1.35,101.9
13,14, C 1.32,110.8
11,15, H 1.090,-121.9
13,16, H 1.09,-121.8
14,17, H 1.09,-129.0
1,18, O -2.022,-50.2,90
1,19, O -2.022,50.2,90
18,20, H -1.21,-128.6
18,21, H -1.28,103.7
19,22, H -1.21,-128.6
19,23, H -1.28,103.7
ZN  2  4 2.010-12.41  4 1.700 -6.53
```

REFERENCES

1. (i) Turner, M. Ph.D. Thesis 1988, McMaster University, 237 pages. (ii) Wang, Z., Ph.D. Thesis 1994, McMaster University, 195 pages.

2. Prince, R. H. Comprehensive Coordination Chemistry Vol. 5 (1987, Oxford, Pergamon) pp. 925-1045.

3. Tang, C. C.; Davalian, D; Huang, P.; Breslow, R. *J. Am. Chem. Soc.* **1978**;*12*:3918-3922.

4. Brown, R. S.; Salmon, D.; Curtis, N. J.; Kusuma, S. *J. Am. Chem. Soc.* **1982**;*11*:3188-3194.

5. Looney, A.; Parkin, G.; Alsfasser, R.; Ruf, M.; Vahrenkamp, H. *Angew. Chem. Int. Ed. Engl.* **1992**;*1*:92-93.

6. Thompson, C. K; Ramaswamy, B.S.; Seymour, E. A. *Can. J. Chem.* **1977**;*55*:877-878.

7. Sigel, H.; Martin, R. B. *Chem. Soc. Rev.* **1994**;*23*:83-91.

8. Lundberg, B. K. S. *Acta Crystallogr.* **1966**;*21*:901-909.

9. Ashby, C. I. H.; Cheng, C. P.; Duesler, E. N.; Brown, T. L. *J. Am. Chem. Soc.* **1978**;*100*:6063-6067.

10. Lehnert, V. R.; Seel, F.; Z. *Anorg. Allg. Chem.* **1980**;*464*:187-194.

11. Wooley, P. *Nature (London)* **1975**;*258*:677-679.

12. Kimura, E; Shiota, T; Koike, T; Shiro, M; Kodam,M. *J. Am. Chem. Soc.* **1990**;*112*:5805-5811.

13. Fersman, A. E. Geokhimiya. Geochemistry Vols I-IV..1933-1939.

14. Widdowson, E.M.; McCance, R. A.; Spray, C.M. *Clin. Sci.* **1951**;*10*:113-125.

15. Prasad, A. S. *Nutr. Rev.* **1983**;*41*:197-208.

16. (i) Bear, M. T. and King, J. C. *Am. J. Clin. Nutr.* **1984**;*39*:556-570. (ii) Endre, L.; Beck, F. W. J.; Prasad, A. S. J. *Trace Elem. Exp. Med.* **1990**;*3*:337-375. (iii) Abu-Hamdan, D.; Migdal, S. D.; Whitehouse, R.; Prasad, A. S.; McDonald, F. D. *Am. J. Physiol.* **1981**;*241*:487-494.

17. Widdowson, E. M.; McCance, R.A.; Spray, C. M. *Clin. Sci.* **1951**;*10*:113-125.

18. Vikbladh, I. Scand. *J. Clin. Lab. Invest.* **1950**;*2*:143-148.

19. (i) Bertrand, G. and Vladesco, R. C. *R. Acad. Sci.* **1921**;*173*:176-179. (ii) Wee, S.; Neilands, J. B.; Buttner, M. L.; Hemming, B. C.; Haymore, B. C.; Seltharam, R. *Biol. Metals* **1988**;*1*:62-65.

20. Prasad, A. S.; Miale, A.; Farid, Z. Schulert, A. Sandstead, H. H. *J. Lab. Clin. Med.* **1974**;*83*:634-639.

21. (i) Batchelor, R.P.; Fehnel, J. W.; Thomson, R. M.; Drinker, K. R. *J. Ind. Hyg.* **1926**;*8*:322-363. (ii) Kehoe, R. A. *Am. Ind. Hyg. Assoc. J.* **1948**;*9*:66-70. (iii) McCord, C. *P. Ind. Med. Surg* **1960**;*29*:101-107.

22. Bertholf, R. L. Handbook on Toxicity of Inorganic Compounds (1988, New York, Dekker) pp. 788-800.

23. Hilbich, C; Kisters-Woike, B.; Reed, J.; Masters, C.L.; Beyreuther, K. *J Mol Biol* **1991**;*218*:149-150.

24. Tanzi, R. E. *Science* **1994**;*2*:1464-1467.

25. Vallee, B. L. and Falchuk, K.H. *Phys. Rev.* **1993**;*73*:79-118.

26. Vallee, B. L. and Auld, D. S. Matrix Metalloproteinases and Inhibitors: Matrix Supplement 1 (1992, Stuttgart, Fischer).

27. Brown, R.S.; Sander, C.; Argos, P. *FEBS Lett.* **1985**;*186*:271-74.

28. Miller, J.; McLachlan, A. D.; Klug, A. *EMBO J.* **1985**;*4*:1609-1614.

29. Margoshes, M. and Vallee, B. L. *J. Am. Chem. Soc.* **1957**;*79*:4813-4816.

30. Geller, B. L. and Winger, D. R. Arch. *Biochem. Biophys.* **1982**;*213*:109-117.

31. (i) Brooks, C. L.; Karplus, M.; Pettitt, B. M. Proteins: A Theoretical Perspective of Dynamics, Structure, and Thermodynamics. Advances in Chemical Physics Vol. LXXI (1988, New York, John Wiley & Sons). (ii) McCammon, J. A.; Harvey, S. C. Dynamics of Proteins and Nucleic Acids (1987, New York, Cambridge University Press).

32. Blundell, T. L.; Johnson, L. N. Protein Crystallography (1976, New York, Academic Press).

33. (i) Prince, R. H. *Adv. Inorg. Chem. Radiochem.* **1979**;*22*:349-346. (ii) Bauer, C.; Gros, G; Bartels, H. Biophysics and Physiology of Carbon Dioxide (1980, New York, Springer-Verlag). (iii) Sigel, H., Metal Ions in Biological Systems, Vol. 15 (1983, New York, Marcel Dekker).

34. Stein, P. J.; Merrill, S. P.; Henkens, R. W. *J. Am. Chem. Soc.* **1977**;*99*:3194-3197.

35. Merz Jr., K. M.; Hoffmann, R.; Dewar, M. J. S. *J. Am. Chem. Soc.* **1989**;*111*:5636-5649.

36. Silverman, D. N.; Lindskog, S. *Acc. Chem. Res.* **1988**;*21*:30-36.

37. Beurger, M. J. X-Ray Crystallography (1942, New York, John Wiley & Sons).

38. Luger, P. Modern X-Ray Analysis of Single Crystals (1980, Berlin, Walter de Gruyter).

39. Stout, G. H. and Jensen, L. H. X-Ray Structure Determination (1989, New York, John Wiley & Sons).

40. North, A. C. T.; Phillips, D. C.; Mathews, F. S. *Acta Crystallogr. A* **1968**;*24*:351-353.

41. Coppens, P.; de Meulenaer, J.; Tompa, H. *Acta Crystallogr.* **1967**;*22*:601-603.

42. Nicolet P3 Diffractometer Manual.

43. Cromer, D. J. and Waber, T. Intl. Tables for X-Ray Crystallography Vol IV (1974, Birmingham, Kynoch Press).

44. Wahren, T. *Acta Chem. Scand.* **1973**;*6*:27-30.

45. Mealli, C. and Maria Proserpio, D. *J. Chem. Ed.* **1990**;*67*:399-402.

46. Tanager Scientific Systems Autotitrator Manual.

47. Brown, I. D. Structure Correlation, Vol. 2 (1994, New York, VCH) Chap 10.

48. Wollam, E. A.; Davidson, W. L.; Shull, C. G. *Phys. Rev.* **1948**;*73*:1348-1351.

49. Freeman, H.C.; Huq, F.; Rosalky, J. M.; Taylor, I. F. *Acta Crystallogr. B* **1975**;*31*:2833-2836.

50. Craven, B.M.; McMullan, R. K.; Bell, I. D.; Freeman, H.C. *Acta Crystallogr. B* **1977**;*33*:2585-2589.

51. McMullan, R. K.; Jordan, T. H.; Jeffrey, G. A. *J. Chem. Phys.* **1967**;*47*:1218-1226.

52. Chion, B.; Charlon, C.; LeBars, C.;Duc, L. *Acta Crystallogr. C* **1984**;*40*:709-711.

53. Kojic-Prodic, B; Ruzic-Toros, Z.; Bresciani-Pahor, N. *Acta Crystallogr. C* **1991**;*47*:1645-1647.

54. Huszthy, P.; Bradshaw, J.S.; Krakowiak, K.E.; Wang, T.;Dalley, N. *J. Het. Chem.* **1993**;*30*:1197-2001.

55. Christianson, D. W. and Alexander, R. S. *J. Am. Chem. Soc.* **1989**;*111*:6412-6419.

56. Woodward, R. B. and Hoffmann, R. The Conservation of Orbital Symmetry (1970, Germany, Verlag Chemie).

57. Craven, B. M.; McMullan, R. K.; Bell, S. D.; Freeman, C. *Acta Crystallogr. B* **1977**;*33*:2585-2589.